HHS Public Access

Author manuscript

Cell Rep. Author manuscript; available in PMC 2025 June 20.

Published in final edited form as:

Cell Rep. 2025 May 27; 44(5): 115728. doi:10.1016/j.celrep.2025.115728.

An integrated proteomics approach identifies phosphorylation sites on viral and host proteins that regulate West Nile virus infection

Zachary Walter[1,10], **Minghua Li**[2,10], **Melissa Molho**[1], **Lauren Berish**[1], **Andrew Isopi**[1], **Mary O'Mara**[1], **Mark Dittmar**[3], **Chike Nwaezeapu**[1], **Alicia Richards**[4,5], **Martin McCullagh**[6], **Nevan J. Krogan**[4,5,7], **Sara Cherry**[3,*], **Jeffrey R. Johnson**[8,9,*], **Holly Ramage**[1,11,*]

[1]Department of Microbiology and Immunology, Thomas Jefferson University, Philadelphia, PA 19107, USA

[2]Department of Pathology, University of Texas Medical Branch, Galveston, TX 77555, USA

[3]Department of Pathology and Laboratory Medicine, University of Pennsylvania, Philadelphia, PA 19104, USA

[4]Department of Cellular and Molecular Pharmacology, University of California, San Francisco, San Francisco, CA 94143, USA

[5]Quantitative Biosciences Institute (QBI), University of California, San Francisco, San Francisco, CA 94143, USA

[6]Department of Chemistry, Oklahoma State University, Stillwater, OK 74078, USA

[7]The J. David Gladstone Institutes, San Francisco, CA 94158, USA

[8]Department of Microbiology, Icahn School of Medicine at Mt. Sinai, New York, NY 10029, USA

[9]Global Health and Emerging Pathogens Institute, Icahn School of Medicine at Mount Sinai, New York, NY 10029, USA

[10]These authors contributed equally

[11]Lead contact

SUMMARY

*Correspondence: cherrys@pennmedicine.upenn.edu (S.C.), jeffrey.johnson@mssm.edu (J.R.J.), holly.ramage@jefferson.edu (H.R.).

AUTHOR CONTRIBUTIONS

H.R. performed WNV infections for MS analysis. J.R.J. and A.R. performed MS. J.R.J. performed proteomic scoring and bioinformatics analyses. H.R. and M.D. performed overexpression studies. H.R., M.L., and M.D. performed immunostaining and microscopy. H.R., M.L., M.D., Z.W., M. Molho, and L.B. performed RNAi and viral infections. H.R., M.L., C.N., L.B., M.O., and Z.W. performed quantitative RT-PCR and western blotting. C.N., A.I., and Z.W. performed site-directed mutagenesis. Z.W. performed NS2b/3 cleavage assays. H.R., M.L., C.N., M. McCullagh, and Z.W. performed data analysis and visualization. A.I. performed multiple alignment analysis for flavivirus proteins. Z.W., A.I., M.O., and L.B. performed WNV replicon assays. Z.W. performed protein purification, *in vitro* ATPase activity, entry, replication, and translation assays. H.R., S.C., J.R.J., and M. McCullagh supervised the research. H.R., S.C., J.R.J., and Z.W. wrote the manuscript with input from M.L and M. McCullagh.

DECLARATION OF INTERESTS

The authors declare no competing interests.

Upon infection, viruses alter the proteome, creating a hospitable environment for infection. Cells respond to limit viral replication, including through protein regulation by post-translational modifications. We use mass spectrometry to define proteome alterations during West Nile virus (WNV) infection. Our studies identify upregulation of HERPUD1, which restricts WNV replication through a mechanism independent of its role in endoplasmic reticulum (ER)-associated degradation (ERAD). We also identify modifications on viral proteins, including a WNV NS3 phosphorylation site that impacts viral replication. Finally, we reveal activation of two host kinases with antiviral activity. We identify phosphorylation at S108 of AMPKβ1, a non-catalytic subunit that regulates activity of the AMPK complex. We also show activation of PAK2 by phosphorylation at S141, which restricts translation of the viral genome. This work contributes to our understanding of the interplay between host and virus while providing a resource to define the changes to the proteome that regulate viral infection.

Graphical abstract

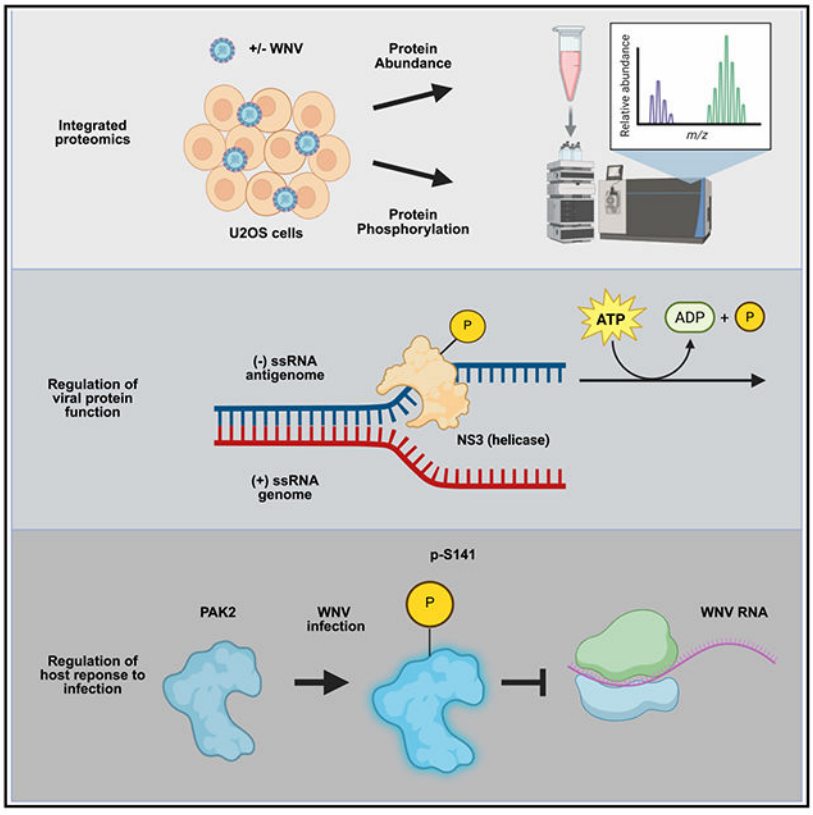

In brief

Walter et al. used proteomics to investigate changes to protein abundance and post-translational modification during West Nile virus infection. Upregulated proteins like HERPUD1 function to restrict viral infection, while phosphorylation on the viral enzyme NS3 and the host kinase PAK2 regulates RNA replication and viral genome translation, respectively.

INTRODUCTION

West Nile virus (WNV) is a neurotropic virus of the *Orthoflavivirus* genus, transmitted to humans by mosquitoes. WNV was introduced into the United States in 1999 and has since become endemic, causing yearly outbreaks associated with disease.[1–3] Flaviviruses are positive-sense RNA viruses with genomes of ~11 kb that are translated as a polyprotein and processed into structural (capsid, prM, and Env) and non-structural (NS1, NS2A, NS2B, NS3, NS4A, NS4B, and NS5) proteins. Given their minimal genomes, flaviviruses utilize host machinery to replicate and subvert antiviral responses. Previously, we used mass spectrometry (MS) to identify host factors interacting with WNV proteins to influence infection.[4] However, this approach did not define changes in protein abundance or modifications that may regulate infection. Protein abundance changes are often inferred by transcriptional data; however, studies show that many proteins are regulated post-transcriptionally, including during infection.[5–16] Moreover, post-translational modifications (PTMs) are an important mechanism to rapidly regulate protein function.[10,17–20] Although flaviviruses do not encode enzymes mediating PTMs, increasing evidence indicates that viruses have evolved to indirectly affect the host PTM machinery to promote infection.[21] Additionally, viral proteins can be modified, and recent discoveries suggest that PTMs can impact viral protein activity.[17,22–28] Our understanding of PTM-mediated protein regulation during WNV infection is limited. While recent work suggests that specific PTMs can affect infection outcomes, comprehensive studies are lacking and can inform the mechanisms underlying viral and host protein regulation.[10,20,26,29] A better understanding of the PTMs that regulate viral protein function will reveal regulatory networks and inform new strategies for interventions.[23,30,31] To this end, we performed an integrated proteomics study to monitor changes in protein abundance and phosphorylation in WNV-infected cells.

RESULTS

Quantitative analysis of protein abundance and phosphorylation during WNV infection

To characterize changes in protein abundance and phosphorylation during WNV infection, we used shotgun proteomics on WNV-infected and uninfected U2OS cells, a human osteosarcoma cell line frequently used to study *Orthoflaviviruses*[4,32–37] (Figure S1A). Trypsin-digested lysates were subjected to liquid chromatography and MS (LC-MS) for protein abundance analysis. Separate aliquots were subjected to phosphopeptide enrichment by an Fe^{3+} immobilized metal affinity chromatography (Fe^{3+}-IMAC) approach followed by LC-MS analysis (Figure 1A).[38,39] Raw MS data were analyzed with the MaxQuant algorithm to identify proteins, localize phosphorylation sites, and extract MS intensity information (Figure 1B). Quality control analyses showed consistent numbers of proteins and phosphosites quantified across the four independent biological replicates (mock vs. infected) (Figures S1B–S1E). Sample correlation and principal components analyses of log2 intensity profiles from WNV and mock-infected samples showed that samples cluster with biological replicates of the same condition (Figures S1F–S1I). The data were analyzed by MSstats to create models of variability, estimate log2 fold change (log2FC), perform significance testing, and adjust for multiple testing.[40] In total, we quantified the abundance of 5,865 protein groups and 10,026 phosphorylation site groups on 3,023 protein groups

(Figure 1B; Tables S1 and S2). “Phosphosite group” refers to modified residues identified on peptides with sequences that are unique for a single protein or shared across a group of homologous proteins. Phosphosite groups separate phosphosites identified on singly, doubly, or triply phosphorylated peptides. The total for unambiguous protein groups identified in all analyses was 5,865 (Figure 1B; Tables S1 and S2). Of the 870 proteins with significantly changed phosphosites, only 14 (1.6%) had concomitant significant changes in protein abundance (Figure 1C), suggesting that the majority of phosphosite changes were independent of protein abundance, consistent with our findings for all protein and phosphosite groups (Figure S2).

We assessed significant changes in host protein abundance by comparing peptides identified from WNV-infected and uninfected cells using a volcano plot (log2FC in abundance of >0.8 or < −0.8, adj. $p < 0.05$) (Figure 1D), identifying 82 host protein groups with increased and 95 protein groups with decreased abundance (Figure 1D; Table S1). A gene ontology (GO) enrichment analysis of the upregulated protein terms revealed pathways including innate immune signaling, mitochondrial depolarization, and RNA polymerase (Pol) I activity (Figure 1E, bottom; Table S3), while downregulated protein terms revealed a decrease in extracellular matrix and collagen organization, consistent with previous findings[41] (Figure 1E, top; Table S3).

Our phosphoproteomics analysis revealed 10,026 phosphosites on 3,023 protein groups (Figure 1B; Table S2). To define changes in host protein phosphorylation during WNV infection, we identified peptides that mapped to a single protein and constructed a volcano plot (Figure 1F; Table S2). In total, we identified 241 differentially increased and 524 differentially decreased phosphosites (log2FC of >1 or < −1, with an adj. $p < 0.05$) during WNV infection. GO analysis of proteins with increased phosphorylation revealed an enrichment in terms involved with proteostasis, including protein chaperones and endoplasmic reticulum (ER)-associated ubiquitin-dependent processes, among other categories relating to the innate immune response (Figure 1G, bottom; Table S4). An analysis of the proteins with decreased phosphorylation showed a significant enrichment in factors comprising the cytoskeleton (Figure 1G, top; Table S4).[42–44] Our analysis of phosphorylation of WNV proteins from infected cells also revealed eight sites of modification across four viral proteins (capsid, prM, NS3, and NS5) (Figure 1H).

Changes in host protein abundance during WNV infection

One significantly enriched set of upregulated proteins belongs to the innate immune response to virus, including interferon-stimulated genes (ISGs) induced by type I interferons (IFNs) (Figure 1E; Tables S1 and S3).[45] We compared our proteins with significantly increased abundance to a set of 57 previously identified ISGs with confirmed antiviral activity in RNA virus infection.[46] Plotting the log2FC of each of these proteins in WNV-infected vs. uninfected cells against the log10 adj. p value revealed that five ISGs (IFIT1, *DDX58* (RIG-I), ISG15, IFIT3, and IFIT5) were significantly increased (log2FC > 0.8, adj. $p < 0.05$) (Figure 2A; Table S5). To gain a broader view of the overlap with previously reported ISGs, we included proteins with a log2FC > 0.5 (adj. $p < 0.05$, 193 proteins total) and compared these with a larger group of 359 ISGs.[47] Again, the overlap between these

datasets was limited to the same five proteins (Figure 2B; Table S5). We validated these findings by western blot with lysates from WNV-infected and uninfected cells for the two most significantly upregulated ISGs, RIG-I (DDX58) and IFIT1 (Figure 2C), and validated the expression of additional upregulated non-ISG candidates, including HSPA6 (protein folding chaperone) and HERPUD1 (ER-associated Ub-dependent process) (Figures 1D and 2D; Table S1).

The transcripts for most proteins with increased abundance are not canonical ISGs.[48] These factors may be induced transcriptionally in response to another stimulus or induced post-transcriptionally. To test this, we selected the 15 most upregulated non-ambiguous proteins and used RT-qPCR to determine if the corresponding transcripts were upregulated during WNV infection (Table S5). We confirmed the transcriptional induction of the known ISGs on this list (IFIT1, DDX58, and ISG15) (Figure 2E). Surprisingly, the majority of the non-ISGs were not induced transcriptionally (Figure 2F). An exception was HERPUD1, which was modestly (2.5-fold) increased (Figure 2F). HERPUD1 expression is induced by ER stress, which occurs during flavivirus infection.[49,50] Together, these data suggest that many of the proteins induced during WNV infection are not encoded by ISGs and that a subset of these proteins are regulated post-transcriptionally.

Overexpression screen identifies antiviral factors

The ISGs upregulated in response to WNV infection are known to have antiviral activity (e.g., RIG-I and IFIT1).[51] However, the functions of the other induced proteins in WNV infection are largely unknown. We performed an overexpression screen to determine if additional upregulated proteins affect flavivirus infection. For this screen, we limited our analysis to host factors with increased abundance and a cutoff of log2FC > 1 and an adjusted $p < 0.05$ and excluded ambiguous host factors (peptides mapping to more than two proteins), for a total of 40 proteins (Table S6). Thirty of these 40 factors were available in our in-house cDNA overexpression libraries (Table S6).

We ectopically expressed each of these proteins in HEK293T cells and infected the cells with WNV Kunjin.[52] As negative controls, we included an empty vector and a vector expressing β-actin. As a positive control, we included an IFIT1-expressing vector.[53,54] After 24 h, we used automated microscopy to quantify infection and calculated the robust Z score for each protein (Figure 3A; Table S6), excluding four factors that led to cellular toxicity when overexpressed (CTU2, LIMA1, PDD2L, and PYRD, <70% cell count of control). Expression of our positive control, IFIT1, resulted in a modest antiviral phenotype (average robust Z score of −0.81 [WNV] and −1.4 [dengue virus; DENV]), consistent with previous studies.[55,56] We used a robust Z score cutoff of ≤ −1.5 to identify three proteins that restricted WNV Kunjin infection, CD44, HERPUD1, and RAP1B (Figure 3A; Table S6), and confirmed RNA and protein expression for each factor (Figures S3A and S3B). We expanded this screen to DENV (NGC serotype 2) to identify factors that impact infection with multiple flaviviruses. Expression of all three of these proteins (CD44, HERPUD1, and RAP1B) also decreased DENV infection (Figure 3A; Table S6). We identified one additional protein, Cyclin H (CCNH), that inhibited DENV infection but did not meet our cutoff (Z

score ≤ −1.5) for WNV. We identified one protein, SESN2, an intracellular leucine sensor, that led to increased infection by both flaviviruses (Figure 3A; Table S6).

We expanded these studies to WNV (NY2000) and found that only expression of HERPUD1, an ER-resident protein, attenuated replication by RT-qPCR (Figure 3B). To confirm the antiviral role of HERPUD1, we used RNAi-mediated depletion and confirmed knockdown by western blotting (Figure S3C). Infection of HERPUD1-knockdown cells resulted in increased WNV and DENV RNA by qPCR, confirming the antiviral activity (Figure 3C). We tested the related flavivirus Zika virus (ZIKV) and found a similar increase in infection upon depletion of HERPUD1 (Figure S3D). Thus, HERPUD1 is upregulated during WNV infection and restricts the replication of multiple flaviviruses.

HERPUD1 is a stress-responsive ER protein implicated in ERAD, a quality control pathway that targets misfolded proteins for degradation.[57–59] Previous studies found that ERAD promotes flavivirus infection, in contrast to the antiviral role of HERPUD1 observed here.[10,60–64] To further explore this, we used small interfering RNAs (siRNAs) to deplete VCP, an ATPase required for ERAD. VCP knockdown reduced WNV replication in U2OS cells (Figures 3D and S3E). Treatment with a chemical inhibitor of VCP (Eey1) reduced WNV infection without impacting cell viability (Figures 3E and S3F). Within ERAD, HERPUD1 interacts with the E3 ubiquitin ligase SYVN1 to facilitate degradation of luminal substrates through the ERAD-L pathway.[65] To test the specific role of ERAD-L, we depleted SYVN1 using siRNAs or chemical inhibitors (LS-102).[66] Depletion or inhibition of SYVN1 led to a decrease in WNV infection without impacting cell viability (Figures 3F, 3G, S3G, and S3H). These data are consistent with a proviral role for ERAD-L in flavivirus infection.

Together, these data suggest a role for HERPUD1 that is distinct from ERAD. To confirm this, we depleted HERPUD2, which is partially redundant with HERPUD1 in ERAD-L.[57,65,67] While HERPUD1 is induced by cellular stress, HERPUD2 is constitutively expressed (Table S1). We reasoned that, if HERPUD1 is antiviral through the ERAD-L pathway, depletion of HERPUD2 should have a similar effect. However, depletion of HERPUD2 did not impact WNV infection (Figures 3H and S3I). These data suggest that the antiviral activity of HERPUD1 is independent of the proviral ERAD pathway. To further characterize the role of HERPUD1, we deleted the N-terminal ubiquitin-like and the SYVN1/UBQLN1 interacting regions (Δ200), which are involved in ERAD function (Figure 3I). We co-transfected wild-type (WT) or truncated HERPUD1 with a WNV replicon and measured viral RNA replication using RT-qPCR. We found that deletion of the N-terminal ERAD-associated domains of HERPUD1 potentiated the antiviral phenotype of HERPUD1 (Figures 3J and S3J). As the C-terminal region of HERPUD1 is not known to facilitate ERAD function, these data further support that the antiviral activity of HERPUD1 is independent of the ERAD pathway.

Phosphorylation sites on WNV proteins

Our phosphoproteomics strategy identified phosphorylation sites on viral proteins. We limited our analyses to those sites that were present in all infected replicates and absent in all mock-infected replicates, totaling eight phosphorylation sites across four WNV proteins. These included two sites in the WNV capsid, one site in prM, two sites in NS3, and

three sites in NS5 (Figure 1H). Of these sites, three have been reported[68,69] (capsid S83, NS5 S3417, and NS5 S3418), while five have not been previously described (capsid S26, prM S216, NS3 S1777, NS3 S1972, and NS5 S3033). To assess the conservation of phosphorylated residues among flaviviruses, we performed a multiple alignment analysis (Figure S4; Data S1). All modified residues in WNV NY2000 are conserved in WNV Kunjin, while others were conserved to various degrees. These viral phosphorylation events are mediated by host kinases, since no WNV protein has kinase activity; therefore, we reasoned that these modifications may constitute a host response to facilitate or inhibit viral replication.

We focused on WNV proteins with enzymatic domains, NS3 and NS5, to determine if phosphorylation affects viral replication. NS5 encodes methyltransferase and RNA-dependent RNA Pol activity, which are both required for viral RNA replication,[70] though all three phosphorylation sites in NS5 were in interdomain regions (Figure 4A). To test whether NS5 phosphosites were important for viral replication, we generated phospho-null (S → A) and phospho-mimetic (S → D) mutations in the NS5 gene of a viral subgenomic replicon construct encoding a green fluorescent protein (GFP) reporter.[71] As a positive control, we generated a D3196A substitution to abrogate the RNA-dependent RNA Pol function of NS5 (Figure 4B).

We found that phospho-mimetic substitutions at two sites (S3033D and S3418D) significantly reduced WNV replicon RNA (Figure 4B). Despite its proximity to S3418, substitution of S3417 had no effect on replication. We scored GFP^+ cells and found significantly decreased GFP expression for both mutants, without impacting cell count (Figures S5A and S5B). These data also indicated a modest decrease in GFP expression in the S3417A replicon (Figure S5A). We next investigated whether NS5 substitutions affected protein abundance by generating mutations in an NS5 expression vector and transfecting WT and mutant vectors into HEK293T cells. Among the mutant proteins, only S3033D had reduced abundance (Figure 4C). We treated WT and S3033D-transfected HEK293T cells with DMSO or compounds to inhibit proteasomal (MG132 or bortezomib) or lysosomal (bafilomycin a1) degradation and did not observe an increase in NS5 S3033D protein, suggesting that the decreased abundance is not mediated by these degradative pathways (Figure S5C). Further experimentation is required to determine whether the RNA encoded by WNV NS5 S3033D is destabilized or is translated at decreased levels.

We next investigated the mechanism of decreased RNA replication for the S3418D mutant. S3418 is in a C-terminal α helix of NS5, near two residues that have been shown to regulate nuclear import in the related DENV, which is required for viral replication.[72,73] To test whether S3418 impacts NS5 nuclear import, we transfected WT and mutant NS5 and separated lysates into cytosolic and nuclear fractions. We did not observe a difference in nuclear localization between WT or mutant NS5, suggesting the replication defect of the S3418D mutant is not attributed to altered localization (Figure S5D). Together, these data show that specific NS5 phosphorylation events can have an inhibitory effect on viral RNA replication.

We also identified phosphorylation sites in WNV NS3 in the ATP-binding (S1777) and RNA helicase (S1972) domains (Figure 4D). The NS2b/3 polyprotein has protease activity and cleaves the junction between NS2b and NS3. To determine if NS3 substitutions affect protein abundance or function, we assessed NS2b/3 protease activity using WT and phospho-mutant vectors. As a positive control, we included a protease catalytic mutant, NS3 S1640A. We used immunoblotting to measure NS2b/3 cleavage in transfected cells and found that the protease-dead control did not cleave the NS2b/3 polyprotein, while WT and phospho-mutant NS3 efficiently processed NS2b/3 (Figure 4E). WNV NS3 also encodes ATPase and RNA helicase activity, both of which are required for viral RNA replication. To determine if these phosphosites affect viral RNA replication, we generated phospho-mutants in the WNV replicon and measured viral RNA replication using RT-qPCR, including the NS3 S1640A and NS5 D3196A controls[71] (Figure 4F). As expected, we observed minimal replicon RNA from our control vectors. The NS3 phospho-mimetic mutations (S1777D and S1972D) and one phospho-null mutation (S1777A) had no effect on replication as compared to WT (Figure 4F). However, one phospho-null mutation (S1972A) significantly reduced the abundance of replicon RNA (Figure 4F). We confirmed this phenotype using microscopy to quantify GFP reporter expression (Figures 4G, 4H, and S5E).

We next examined S1972 using a crystal structure of WNV NS3 (PDB: 2QEQ).[74] While S1972 is in the helicase domain of NS3, it is in close proximity to the ATP-binding pocket, near N1922 (15.75 Å CA-CA distance) in NS3 motif V, G1702 (13.21 Å CA-CA distance) in NS3 motif I, and R1969 (8.90 Å CA-CA distance) in NS3 motif VI (Figure 4I). Motifs I and VI are involved in ATP binding, while motif V is involved in energy transduction.[75,76] To determine whether S1972 regulates NS3 ATPase activity, we purified WT, S1972A, and S1972D versions of the WNV NS3 helicase domain (NS3h) and performed an *in vitro* ATPase assay[77] (Figure S5F). As a control, we also purified an A1792L mutant, which disrupts the DEAH catalytic motif of NS3h.[75]

We measured V_0 of ATP hydrolysis at a range of substrate concentrations and calculated K_m and k_{cat} by fitting the data to the Michaelis-Menten equation using non-linear regression in GraphPad Prism (Figures 4J and 4K). Compared to WT, A1792L NS3h had an increased K_m and decreased k_{cat}, with significantly decreased catalytic efficiency (k_{cat}/K_m). We anticipated that S1972A NS3h may have impaired ATPase activity due to its replication phenotype; however, we observed a significant increase in catalytic efficiency, with a decreased K_m and an increased k_{cat} compared to WT. The phosphomimetic substitution at this site, S1972D, had a K_m similar to that of the WT protein, with a modest increase in k_{cat} and overall similar catalytic efficiency. Together, these results suggest that WNV S1972 may be important for NS3h activity through interactions with the ATP-binding pocket to regulate viral RNA replication. Our combined WNV NS3 and NS5 data demonstrate that phosphorylation of viral proteins can have both negative and positive regulatory roles in viral RNA replication.

Changes in host protein phosphorylation upon WNV infection

We observed significant alterations to host protein phosphorylation during WNV infection Table S2). Phosphorylation can activate kinases, and we identified phosphorylation events

on multiple kinases during WNV infection. Therefore, we investigated significantly regulated kinases based on our phosphoproteome data. First, we used the Kinase Library to identify kinase motifs enriched in up- or downregulated phosphosites (Figure 5A, left; Table S7).[78] Next, we applied the kinase-substrate enrichment analysis (KSEA) algorithm to infer changes in kinase activities (Figure 5A, middle; Table S8).[79] Kinase Library analysis predicted that 63 kinases were downregulated with an adjusted $p < 0.05$, while no kinases were predicted to be upregulated with the same criteria. KSEA did not predict any kinase regulation using the adjusted p value cutoff of <0.05. Using a p value (unadjusted) cutoff of <0.05, we found 15 kinases predicted to be downregulated (including PKC orthologs and MAP kinases) and 2 kinases (MAPKAPK2 and PAK4) predicted to be upregulated (Figure 5A, middle; Table S8). Finally, we cross-referenced our significant phosphosite changes (log2FC >1 or < −1 and an adjusted $p < 0.05$) with the PhosphoSitePlus database to identify known regulatory phosphorylation events (Figure 5A, right; Table S9).[80] We also included those sites with peptides matching to a single protein that were absent in all four replicates of one condition and present in all four replicates of the other condition (Table S2), identifying 62 regulatory phosphosites on 56 proteins (Figure 5A, right; Table S9). Of these, 15 are predicted to increase, while 7 are predicted to decrease protein activity (Figures 5A and 5B; Table S9). Importantly, this strategy identified a known regulatory phosphorylation site on a canonical antiviral restriction factor, STAT1. We also observed an increase in phosphorylation on other proteins linked to viral restriction, including BCL10 and p53 (Figure 5B).[81–85]

We reasoned that additional regulatory phosphosites in this dataset may be important for WNV infection and further explored these candidates, focusing on phosphorylation events predicted to increase protein activity (Figure 5B). These included an increase in phosphorylation of seven “activating” phosphosites and a decrease in phosphorylation of eight “inhibitory” phosphosites. We validated these data by immunoblotting for four proteins with phosphosites that were upregulated and for which phospho-antibodies were commercially available (STAT1 [pS727], c-JUN [pS63], AMPKβ1 [pS108], and PAK2 [pS141]) and confirmed phosphorylation upon WNV infection without a change in abundance (Figure 5C).

The AMP-activated protein kinase (AMPK) complex is composed of three subunits (α1-2, β1-2, and γ1-3) and regulates metabolism, stress responses, and growth.[86] AMPK activation through AMPKα-Thr172 phosphorylation has been observed during diverse viral infections.[87–90] AMPKβ can regulate the activity of the complex, with S108 phosphorylation increasing kinase activity.[88,91–94] Studies have suggested divergent roles for AMPK in flavivirus infection and no known role for modulation of AMPKβ during any viral infection.[89,90,95–97] Therefore, we explored the role of AMPK during WNV infection. First, we found increased AMPKα-Thr172 phosphorylation, as reported for other viral infections (Figure S6A). To test the role of the AMPK complex, we infected WT and AMPKα1/2-knockout mouse embryonic fibroblasts (MEFs) with WNV NY2000 and observed a significant increase in WNV infection in the absence of AMPKα (Figures S6B and S6C). We further tested whether AMPK impacts ZIKV or DENV and found a similar phenotype (Figure S6C). Together, these data demonstrate an antiviral role for the AMPK complex in flavivirus infection.

While either AMPKβ subunit (AMPKβ1 or AMPKβ2) can form an AMPK complex, S108 phosphorylation is specific to AMPKβ1.[91] A role for AMPKβ1, or S108 phosphorylation, has not been described during viral infection. To determine if AMPKβ1 plays a specific role in flavivirus infection, we silenced AMPKβ1 in U2OS cells and observed significant knockdown of AMPKβ1, but not AMPKβ2 (Figure S6D). We infected these cells with WNV and observed increased viral replication (Figure 5D) and confirmed these data using immunoblotting (Figure 5E). WNV is neurotropic, infecting multiple cell types in the central nervous system[98]; thus, we explored the role of AMPK in the astrocytoma cell line CCF-STTG1 and cerebral microvascular endothelial cell line HBEC-5i. We observed antiviral activity for AMPKβ1 in both cell lines (Figures 5F and S6G). We next performed a $TCID_{50}$ assay and also observed increased WNV titers (Figures 5G and S6H). These data demonstrate that AMPK restricts WNV infection in multiple cell types.

Previous studies have demonstrated antiviral activity for AMPK via an inhibitory acetyl-CoA carboxylase (ACC) phosphorylation[95,99–101] or an activating TBK1 phosphorylation event.[102] To determine if AMPK functions through either of these mechanisms in WNV infection, we immunoblotted lysates from uninfected or WNV-infected, AMPKβ1-silenced U2OS cells. We observed a modest increase in ACC phosphorylation during WNV infection, which was not affected by AMPKβ1 depletion, and TBK1 phosphorylation did not change in any condition (Figure S6I). Together, these data suggest that phosphorylation and activation of AMPKβ1 may be important for the antiviral activity of AMPK through a mechanism independent of ACC and TBK1.

PAK2 restricts WNV infection

P21-activated protein kinase 2 (PAK2) regulates cell motility, survival, and cytoskeletal dynamics. We identified a phosphorylation event known to activate PAK2 (pSer141) during WNV infection.[103,104] To determine whether PAK2 impacts WNV replication, we silenced PAK2 using siRNAs and confirmed knockdown using RT-qPCR (Figure S7A). We infected these cells with WNV and observed a significant increase in viral RNA (Figure 6A). We confirmed this antiviral role in CCF-STTG1 and HBEC-5i cells, as measured by viral RNA and infectious virions (Figures 6B–6E, S7B, and S7C). We expanded our studies to DENV and ZIKV infection in U2OS cells and found that PAK2 can restrict infection of multiple flaviviruses (Figures 6F, S7D, and S7E).

Since PAK2 is involved in regulating cytoskeletal dynamics during some viral infections,[19,105] we reasoned that PAK2 may impact WNV entry.[106] To test this, we performed a viral entry assay in U2OS cells and found that PAK2 depletion did not affect entry (Figure 6G). Next, we synchronized infection at a high MOI and observed a divergence in viral RNA abundance between control and PAK2-depleted cells beginning at 9 h post-infection, near the onset of viral RNA replication (Figure 6H). To test whether PAK2 affects ongoing RNA replication, we silenced PAK2 in HEK293T cells harboring an integrated WNV replicon that stably produces viral RNA and found that ongoing replication was unaffected, suggesting that PAK2 impacts a step prior to the establishment of replication organelles (Figures S7F and S7G).

Formation of replication organelles is dependent on viral proteins produced from the pioneer round of cap-dependent translation from the viral RNA genome. PAK2 can inhibit cap-dependent translation[107]; therefore, we performed a translation assay to determine if PAK2 affects viral genome translation. We generated a D3196A RdRp-null substitution into a DNA-launched WNV replicon encoding *Renilla* luciferase and transfected this into PAK2-depleted 293T cells along with the WT replicon.[71] As expected, we found that the Pol-dead D3196A reporter signal was significantly lower than that of WT (Figure S7H). However, the Pol-dead replicon displayed accumulating luciferase activity over time, consistent with ongoing translation of promoter-driven transcripts from the plasmid (Figure S7H). As a positive control, we treated cells with cycloheximide (CHX) and observed a decrease in reporter activity (Figure S7I). Next, we transfected the D3196A replicon into PAK2-silenced HEK293T cells and found that depletion of PAK2 increased translation of the luciferase reporter (Figure S7J).

As PAK2 is antiviral for DENV, we assessed whether PAK2 also restricts translation in this virus. We used a replication-competent and Pol-dead RNA-launched DENV replicon encoding *Renilla* luciferase.[108] First, we confirmed the antiviral role for PAK2 in the context of the replicon by transfecting capped WT DENV replicon RNA[108] into PAK2-silenced cells and found a significant increase in reporter activity (Figure 6I). Next, we tested translation using the Pol-dead DENV replicon construct.[108] As a control, we transfected cells with a capped Pol-dead DENV replicon, treated with CHX, and observed decreased reporter activity (Figure S7K). We next transfected the Pol-dead DENV replicon into PAK2-silenced cells and found increased viral translation (Figure 6J). As we propose that PAK2 restricts viral replication via inhibition of cap-dependent translation, we reasoned that PAK2 would not restrict the related hepatitis C virus (HCV), which uses an internal ribosome entry site (IRES) for translation.[109] Therefore, we tested the role of PAK2 in HCV infection in Huh7.5 cells (Figure S7L). In contrast to flavivirus infection, PAK2 silencing did not impact HCV replication (Figure 6K). Taken together, our data show that PAK2 is activated via phosphorylation at S141 during WNV infection and restricts flaviviruses via inhibition of cap-dependent translation of the viral RNA genome.

DISCUSSION

Integrated proteomics approaches that combine protein abundance and PTM datasets have been previously used to discover factors and modifications that affect infection for a handful of viruses.[10,19,31] However, an approach to monitor changes in protein abundance and phosphorylation has not been applied to WNV. To address this gap, we characterized changes in global protein abundance and regulation by phosphorylation during WNV infection and discovered both antiviral factors and regulatory modifications that influence viral replication. Our MS approach revealed an enrichment in canonical antiviral and IFN-stimulated proteins; however, most upregulated proteins we identified are not associated with antiviral defense. The five ISGs we found to have increased abundance are consistent with a recent study suggesting that only a subset of ISGs acts as antiviral effectors in a given infection.[110] This further suggests that translational profiling during infection can reveal the downstream effectors important for controlling infection. We detected several other proteins with increased abundance during infection and reasoned that some may be

IFN-independent antiviral factors. Indeed, our overexpression screen revealed an antiviral phenotype for HERPUD1, an ER-resident protein involved in ERAD.[59,65,111] However, our data suggest that the antiviral role of HERPUD1 is independent of its function in ERAD. HERPUD1 was previously found to interact with DENV NS4b, which may influence the antiviral activity of HERPUD1 during flavivirus infection or serve to recruit mediators of this antiviral activity.[35]

We performed phosphoproteomic experiments to identify phosphorylation events during WNV infection. PTMs on viral proteins provide a rapid, reversible mechanism to modify function during different stages of the viral life cycle.[26,112–115] These “molecular switches” may allow a single viral protein to play multiple roles throughout the infectious cycle, a critical strategy for viruses with a limited coding capacity. We identified eight phosphorylation sites across four WNV proteins, including three previously reported sites.[28,68,69] We focused on phosphorylation of the two non-structural proteins with enzymatic activity, NS3 and NS5. We identified two serine residues in NS5 that inhibit viral RNA replication when substituted with the phosphomimetic aspartate. In HCV, the viral NS5a protein is hyperphosphorylated to regulate NS5a function during establishment of replication organelles,[116] viral RNA replication,[112] and virion production.[113] Our data suggest the possibility of a related mechanism in mosquito-borne flaviviruses, where phosphorylation could negatively regulate RNA synthesis and facilitate virion packaging. Further experimentation is required to mechanistically define the impacts of WNV NS5 phosphorylation on viral RNA replication and the viral life cycle.

We also identified a phosphorylated residue on WNV NS3 (S1972) and show that a phospho-null substitution inhibits RNA replication. Interestingly, this mutant protein hydrolyzes ATP with higher efficiency than WT, suggesting that phosphorylation of WNV S1972 modulates ATPase activity. While these results were unexpected, they are consistent with a previous study showing that substitutions in the DENV NS3 helicase increased ATP hydrolysis but impaired overall helicase activity, possibly due to alterations in the flexibility of the ATP-binding pocket.[117] These data suggest that the ATPase and helicase activities of the *Orthoflavivirus* NS3 protein are tightly coupled and finely tuned for optimal viral replication. Future studies will further characterize the function of S1972 phosphorylation and explore the mechanisms of NS3 phospho-regulation, including whether previously identified WNV-interacting host kinases mediate viral protein phosphorylation.[4] Taken together, these data suggest that phosphorylation may serve as an important regulatory mechanism during *Orthoflavivirus* infection.

We also identified changes to host protein phosphorylation during infection and focused on phosphosites that regulate the activity of the modified protein. Among these, we discovered a phosphorylation site on S108 of the AMPKβ1 regulatory subunit in the AMPK complex, which has been reported to alter the specificity of an allosteric regulatory pocket on AMPK, the ADaM site.[91,92,94,118] Our data support an antiviral role for the AMPKβ1 subunit distinct from previously described mechanisms.[87,95,99–101,119] It has been demonstrated that AMPKβ1 S108 phosphorylation may be mediated by a kinase other than AMPK during conditions of stress and that phosphorylation of AMPKβ1 S108 may alter target substrate specificity.[93] Further investigation is required to determine the role of β1 S108

phosphorylation in regulating AMPK function and the effect on AMPK substrates during infection.

Finally, we identified an increase in Ser141 phosphorylation on the kinase PAK2. Conditions of stress are known to induce Ser141 phosphorylation, directing PAK2 translocation to the ER and activating kinase activity.[103,104] Depletion of PAK2 results in increased flavivirus replication, demonstrating an antiviral role for this kinase. PAK kinases have been previously implicated in infection with diverse viruses, including a role in viral entry.[105,120,121] While PAK2 depletion did not impact WNV entry, we found that PAK2 depletion enhanced cap-dependent translation of the viral genome. We propose a model where Ser141 phosphorylation activates PAK2, inhibiting viral genome translation and delaying establishment of replication organelles. Given the function of PAK2 in cytoskeletal reorganization, PAK2 may also play a role in other stages of the viral life cycle, such as ER remodeling during viral replication or virion assembly. Future studies will determine the precise mechanism of PAK2 activation and antiviral activity during flavivirus infection.[103]

Taken together, our work uncovers complex layers of regulation for viral proteins and the host response to WNV infection by revealing alterations in protein abundance and phosphorylation. Our abundance data highlight changes that cannot be inferred by monitoring the transcriptional response and uncover post-transcriptionally regulated antiviral proteins. Further, the PTM data presented here identify additional points of regulation for antiviral proteins. Our finding that PTMs on viral proteins impact specific protein functions presents the possibility that these modifications may regulate transitions between stages of the flaviviral life cycle. Finally, our studies complement previously published -omic datasets and inform future research toward understanding mechanisms regulating flavivirus infection.

Limitations of the study

Proteomics has inherent limitations; some proteins or PTMs may not be observed if: (1) their intensities are below the MS detection limit, (2) they do not generate peptides in an optimal size range, or (3) peptides are not efficiently ionized by electrospray ionization, which is poorly understood. Our proteomics data are limited to a single time point in a representative cell line, and the MOIs used for MS sample preparation at this time point likely represent a mixed signature of cells infected during the initial inoculation and cells infected by virions produced from the first round of infected cells. This may broaden our ability to detect changes to protein abundance and phosphorylation but does not allow for the assessment of time-resolved changes during WNV infection. Future studies leveraging synchronized infections across a range of time points and in additional cell types will more comprehensively define the regulation of protein abundance and protein phosphorylation during WNV infection.

The substitutions generated in viral proteins may affect adjacent PTMs on those proteins or may affect viral protein function independent of PTMs. While we showed that S1972A NS3h has increased ATPase efficiency compared to WT, we have not examined helicase or RTPase activity, which may also be affected. Previous data have demonstrated that phosphorylation of PAK2 at S141 and AMPKβ1 at S108 activates the enzymatic activity of these proteins. While we anticipate that these modifications have a similar effect in the

context of WNV infection, further studies are required to confirm this and to determine whether the host factors regulating phosphorylation differ between infected and uninfected cells.

RESOURCE AVAILABILITY

Lead contact

Requests for information and resources should be directed to the lead contact, Holly Ramage (holly.ramage@jefferson.edu).

Materials availability

All reagents generated in this study will be made available upon request.

Data and code availability

The MS proteomics data have been deposited to the ProteomeXchange Consortium via the PRIDE partner repository with the dataset identifier PRIDE: PXD050159; https://proteomecentral.proteomexchange.org/cgi/GetDataset?ID=PXD050159.[122] R code for subsequent analyses is available on GitHub at https://github.com/jrjohns1/Walter-et-al. Additional information required to analyze these data are available from the lead contact upon request.

STAR★METHODS

EXPERIMENTAL MODEL AND STUDY PARTICIPANT DETAILS

Microbe strains: West Nile Virus: Kunjin CH16532 was isolated from an infected Australian mosquito in 1960.

West Nile Virus: NY2000 Crow-3356 isolated from an infected crow in New York, USA in the year 2000. Stocks were grown in C6/36 *Aedes albopictus* cells.

Dengue Virus: Serotype 2 NGC isolated from an infected human in New Guinea in 1944. Stocks were grown in C6/36 *Aedes albopictus* cells.

Zika Virus: Mexico 2016 Mex2-81 was obtained from the World Reference Center of Emerging Viruses and Arboviruses in Galveston, TX, USA.

Cell lines: U2OS: Human osteosarcoma cell line derived from a 15 year old Caucasian female.

HEK293T: Human embryonic kidney cell line derived from a female fetus.

BHK21: Syrian golden hamster kidney fibroblasts derived from five one-day-old baby hamsters (unsexed).

CCF-STTG1: Human astrocytoma cell line derived from a 68 year old Caucasian female.

HBEC-5i: Human microvascular endothelial cell line derived from fragments of human cerebral cortex frommultiple patients transformed by SV40 large T antigen.

C6/36: *Aedes albopictus* mosquito cell line derived from mosquito larvae.

Cell lines were obtained directly from and validated by ATCC and confirmed negative for *Mycoplasma* contamination.

METHOD DETAILS

Cells and viruses: HEK293 and U2OS cell lines were obtained from the American Type Culture Collections. All cultures were grown under standard conditions in Dulbecco's Modified Eagle Medium supplemented with 10% fetal bovine serum, 100 units penicillin, 100 μg streptomycin and 2 mM L-alanyl-L-glutamine dipeptide (GlutaMax, Gibco). HEK293 cells were transfected using X-treme GENE 9 (Roche Applied Science) according to the manufacturer's instructions. U2OS cells were transfected using Fugene HD (Promega) according to the manufacturer's instructions. BHK cells were maintained as previously described.[33] The WNV-KUNV isolate (CH16532) was a generous gift of R. Tesh (World Reference Center of Emerging Viruses and Arboviruses, Galveston, TX) and WNV NY2000 was a generous gift from Michael Diamond. DENV-2 (NGC from BEI), and ZIKV Mexico 2016 (Mex2-81; a generous gift from R. Tesh) were grown as previously described.[123] Viral titers were determined in BHK-21 cells by $TCID_{50}$ assay. The DNA-launched CMV-driven WNV replicon was a gift from Theodore C. Pierson. The RNA-launched wild-type and polymerase-dead DENV replicons were a gift from Jan Carrette.

WNV infection and sample preparation for mass spectrometry: U2OS cells were infected with WNV NY2000 at an MOI of 1 for 20 hours. Following infection, media was aspirated and cells were detached by the addition of cell dissociation buffer (10 mM EDTA in D-PBS). Cell suspensions were transferred to 50 ml conical tubes, pelleted and resuspended in urea lysis buffer (8M urea, 50 mM NH4HCO3, 150 mM NaCl, Complete EDTA-free mini protease inhibitor tablets (Roche, 1 mini tablet per 10 ml buffer). Lysates resuspended in urea lysis buffer were stored at −80° C until further processing. Tris-(2-carboxyethyl) phosphine (TCEP) was added to a final concentration of 4 mM. DNA was sheared via probe sonication, on ice, at 20% amplitude for 20 s., followed by 10 s of rest a total of three times. Following sonication, protein concentration was determined using Bradford assay. Iodoacetamide (IAA) was added to each sample to a final concentration of 10 mM, and samples were incubated in the dark at room temperature (RT) for 30 minutes. Excess IAA was quenched by the addition of dithiothreitol (DTT) to 10 mM, followed by incubation in the dark at RT for 30 minutes. Samples were then diluted with 0.1 M NH4HCO3 (pH = 8.0) to a final urea concentration of 2 M. Trypsin (Promega) was added at a 1:100 (enzyme:protein w:w) ratio and digested overnight at 37C with rotation. Following digestion, 10% trifluoroacetic acid (TFA) was added to each sample to a final pH ~2. Samples were desalted under vacuum using Sep Pak tC18 cartridges (Waters). Each cartridge was activated with 1 mL 80% acetonitrile (ACN)/0.1% TFA, then equilibrated with 3 x 1 mL of 0.1% TFA. Following sample loading, cartridges were washed with 4 x 1 mL of 0.1% TFA, and samples were eluted with 4 x 0.5 mL 50% ACN/0.25% formic acid (FA).

100 μg of each sample was used for protein abundance measurements, and 1 mg was used for phosphopeptide enrichment. Samples were dried by vacuum centrifugation.

Phosphopeptide enrichment: For each sample batch, 400 μL (30 μL per sample) of 50% Superflow bead slurry (QIAGEN) was added to a 2 mL bio-spin column. Beads were incubated with 4 x 500 μL of 100 mM EDTA for 30 s, washed with 2 x 500 μL H2O, incubated 4 x 500 μL with 15 mM $FeCl_3$ for 1 minute, washed 3 x 500 μL H2O, and washed once with 500 μL of 0.5% FA to remove residual Fe^{3+}. Beads were resuspended in 600 μL of H2O and 60 μL were aliquoted into a C18 NEST column that had been equilibrated with 150 μL of 80% ACN, 0.1% TFA. 1 mg of digested peptides were resuspended in 75% ACN/0.15% TFA and incubated with beads for 2 minutes, mixed by pipetting and incubated again for 2 minutes. Beads were washed 4 x 200 μL with 80% ACN, 0.1% TFA, then washed 3 x 200 μL with 0.5% FA, incubated 2 x 200 μL with 500 mM potassium phosphate buffer pH 7 and incubated 2 x 200 μL with 0.5% FA for 15 seconds. Phosphopeptides were eluted by centrifugation at 1000xg for 30 seconds with 2 x 75 μL of 50% ACN, 0.1% FA.

Mass spectrometry data acquisition: All samples were analyzed in technical duplicate on an Orbitrap Lumos mass spectrometry system equipped with an Easy nLC 1200 ultra-high pressure liquid chromatography system (Thermo Fisher Scientific) interfaced via a Nanospray Flex nanoelectrospray source. Samples were injected on a C18 reverse phase column (25 cm x 75 mm packed with ReprosilPur 1.9 mm particles). Mobile phase A consisted of 0.1% FA, and mobile phase B consisted of 0.1% FA/80% ACN. For phosphorylation and protein abundance analyses, peptides were separated by an organic gradient from 5% to 30% mobile phase B over 180 min at a flow rate of 300 nL/minute, then held at 90% B for 120 minutes. The mass spectrometer operated in data-dependent acquisition (DDA) mode by acquiring a full scan over a m/z range of 350-1500 *m/z* in the Orbitrap at 120,000 resolution (@200 m/z), followed by as many MS/MS scans as could be collected in 3s in the Orbitrap at 15,000 resolution. Dynamic exclusion was set to 30 seconds, with a 10 ppm exclusion width setting. Peptides with charge states 2-8 were selected for MS/MS interrogation using higher energy collisional dissociation (HCD) with a normalized collision energy of 30%.

Data processing: Raw mass spectrometry data was analyzed by the MaxQuant algorithm (version 1.6.8.0) to match mass spectra to peptide and protein sequences, localize post-translational modification sites, and extract ion intensity information.[124] The data were searched against the UniProt *Homo sapiens* reference proteome and the UniProt West Nile virus (strain NY-99) reference proteome (both downloaded on October 10, 2019), reviewed sequences and canonical isoforms only. The match between runs feature was enabled with a match time window of 2 min. For protein abundance analysis, variable modifications were considered for methionine oxidation and protein N-terminal acetylation. For phosphorylation analyses, variable modifications were considered for serine, threonine, or tyrosine phosphorylation in addition to the same modifications considered for protein abundance. All other MaxQuant parameters were used at default settings. The data were subsequently analyzed by the MSstats package in R (version 3.22.1).[40] Data were normalized by equalizing medians, the summary method was tukey's median polish (TMP),

the cutoff value for the model was the minimum value for each feature across runs (minFeature), model-based imputation was enabled, and the maximum quantile for deciding censored missing values was 0.999. Conditions were compared using the groupComparison function to estimate Log2-fold-changes, p-values, and p-values adjusted for multiple testing. In some cases, a protein or phosphosite was detected in all four replicates of one condition and absent in all four replicates of the condition for comparison. In these cases, the fold-change was defined as positive or negative infinity, and these data points were considered as significantly up- or downregulated for subsequent enrichment analyses, including GO analysis, kinase library analysis, and KSEA analysis. Any other cases, in which a protein or phosphorylation site was not detected in any replicates of one condition and was detected in fewer than all four replicates of the other condition, were assigned a NA value for fold-change and not included in any subsequent analyses. See data and code availability section for code access.

GO enrichment analysis: Gene Ontology (GO) analysis was conducted using a hypergeometric test with the dhyper function in R (see data and code availability section for code access). Gene ontologies annotations were downloaded from UniProt and GO definitions from the Gene Ontology Resource on 18 February 2021.[125,126] The test set was comprised of proteins significantly increasing or decreasing as defined above in the comparison of interest, and the background set was all proteins quantified in the comparison of interest. Enrichment tests were performed for any GO term that had at least 2 overlapping proteins in the test set. Proteins identified by peptides that were not unique to a single protein sequence were excluded from this analysis. A detailed list of all terms, results and statistics for each analysis are provided in the supplementary data (Tables S3 and S4).

Western blotting to validate protein abundance and phosphorylation: U2OS cells plated into 6-well plates were either uninfected or infected with WNV NY2000 for 16 hours, 20 hours, and 24 hours. Cells were washed with PBS and lysed in RIPA buffer supplemented with protease inhibitor cocktail (Sigma). After incubation on ice for 20 minutes, the cell lysates were clarified by centrifugation at 18,000xg for 10 minutes at 4° C. The clarified cell lysates were then transferred into a new tube and boiled for 10 minutes with 6x sample buffer. Protein samples were separated on 12% SDS-PAGE gels and transferred to PVDF membranes (Millipore). After blocking with 5% milk in TBST, the membranes were incubated with indicated primary antibodies overnight at 4° C. After washing with TBST for 3 times, the membranes were incubated with HRP-conjugated secondary antibodies for 1 hour at room temperature. Western blots were visualized using Amersham Imager 680 (Amersham). The specific primary antibodies used are detailed below.

RNA isolation and quantitative RT-PCR: Total cellular RNA was isolated using Trizol (ThermoFisher Scientific) purified and DNase-treated using RNA Clean & Concentrator (Zymo) per manufacturer's instructions. Complementary DNA (cDNA) was synthesized using 1 μg of input RNA with using random hexamer primers (Life Technologies) with MMLV reverse transcriptase (Invitrogen) in a total volume of 20 μl. cDNA reactions were diluted 1:5 and 20 μl of each diluted sample was used to make a pooled reference. The

pooled reference was used for subsequent 10-fold dilutions to generate a standard curve for all targets being measured. cDNA reactions were further diluted 1:5 (1:25 total dilution) and SYBR green reactions contained 5 μl of 2x Maxima SYBR green/Rox qPCR Master Mix (Thermo), 5 μl of diluted cDNA, 5 pmol of both forward and reverse primers, analyzed by qPCR and the relative abundance of each target was calculated using the standard curve. The relative values for each transcript were normalized to a control RNA (18S rRNA or GAPDH) and compared between experimental conditions. A complete list of primers used for quantitative RT-PCR is provided in Table S13.

cDNA overexpression screen: HEK293 cells were seeded at 25,000 cells/well in 200 μl media per well in collagen-coated 96-well plates for cDNA transfection. A total of 100 ng plasmid DNA was transfected into each well using X-tremeGENE 9 (Sigma) according to the manufacturer's instructions. A GFP-expressing vector was included as a positive control for transfection. After 24 hours, we confirmed GFP expression and proceeded with infections. WNV and DENV infections were done at an MOI of 0.01. Infectivity was measured 24 hours post infection by immunostaining and automated microscopy. Cells were fixed with 4% formaldehyde for 10 minutes, permeabilized with 0.1% Triton X-100 for 15 minutes, washed three times with PBS and blocked with 2% BSA in PBS-T. Cells were stained overnight with the mouse 4G2 (anti-envelope) antibody (1:4000 for DENV and ZIKV, 1:12000 for WNV Kunjin). Cells were washed three times in PBS-T and incubated with 5 μg/mL Hoechst 33432 to identify nuclei and with an Alexa Fluor-488-conjugated α-mouse secondary antibody (1:1000) for one hour at room temperature. Cells were washed three times with PBS-T and imaged in 100 ul PBS. Nine sites per well were imaged at 10X magnification (ImageXpress Micro; Molecular Devices). Each screen was performed in duplicate. Automated image analysis (MetaXpress; Molecular Devices) was used to segment the images and determine the number of DAPI-positive and 488-positive cells. The percentage of infected cells was calculated, averaged for the nine sites in each well, and log transformed. The plate median and interquartile range were calculated and used to calculate a robust Z score for each well using the following equation: [(Log10(%infection) – Log10(median)/(IQR × 0.74)].[127] The robust z-scores for the experimental replicates were average and candidates were identified as positive if the averaged robust Z score was <− 1.5 or >1.5. Cytotoxic candidates were identified based on nuclei counts and those with a >30% decrease in cell number as compared to the average cell count were excluded from further study. The heat map for visualization was generated using Morpheus (https://software.broadinstitute.org/morpheus/). Hierarchical clustering was performed using Euclidean distance. The complete screening results can be found in Table S6.

RNAi, transfection, and infection studies: For RNAi experiments, 200,000 U2OS cells were plated in a 6-well plates and siRNAs were transfected using HiPerFect (Qiagen) according to manufacturer recommendations at a final concentration of 20nM and incubated for 48–72 h. Cells were infected with WNV, DENV or ZIKV at the MOIs and timepoints indicated in the figure legends. Following infection, cells were collected in 1 mL Trizol for quantitative RT-PCR experiments or washed 3X in PBS and resuspended in 1 mL IP buffer for western blotting. For transfection experiments, 200,000 U2OS cells were plated in 6-well plates and the indicated vectors were transfected using Fugene HD (Promega) and incubated

for 48 h. Following transfection, cells were collected in 1 mL Trizol for quantitative RT-PCR experiments or washed 3X in PBS and resuspended in 300 μL RIPA buffer with protease inhibitors for western blotting. A complete list of siRNA sequences is provided in Table S11.

WNV replicon studies and generation of mutants: Site-directed mutagenesis was performed with the CloneAmp HiFi PCR premix and In-Fusion cloning kit (Takara) to generate phospho-null (Ser→Ala) or phospho-mimetic (Ser→Asp) substitutions in a lineage-II WNV replicon encoding a GFP reporter in-frame with the WNV nonstructural proteins 1 through 5[71] (Rep-G/Z). HEK293T cells seeded into 6-well plates were transfected using X-tremeGene9 with 1μg Rep-G/Z plasmid and incubated for 48 h. Cells were replated into 96-well black-walled plates for immunofluorescence and the remainder were collected in Trizol. Quantitative RT-PCR was used to measure viral RNA using primers specific to WNV nonstructural genes.

NS2b/3 cleavage studies: HEK293T cells seeded into 6-well plates were transfected with 1 μg plasmids encoding WNV NS2b/3 wild-type, alanine mutants (S1777A, S1972A) or aspartic acid mutants (S1777D, S1972D), or a protease catalytic mutant S1640A. The transfections were performed using X-tremeGENE 9 DNA Transfection Reagent (Roche) according to the manufacturer's instructions. At 48 hours post-transfection, the transfected cells were collected and lysed in RIPA buffer containing Halt protease inhibitor cocktail (Thermo Scientific). Following centrifugation at 18,000xg for 10 minutes at 4° C, the clarified cell lysates were dissolved in 6x SDS sample buffer and subjected to SDS-PAGE. Expression of WNV NS2b/3 polyprotein and cleaved NS3 was examined using α-Strep antibody (Abcam). A specific antibody against WNV NS2B (GeneTex) was used to determine the cleavage of WNV NS2B from NS2b/3.

Protein purification: Protein purification was performed as previously described.[77] Briefly, an IPTG-inducible vector encoding the helicase domain of WNV NS3 (residues 1676-2124) was used as a template for site-directed mutagenesis (Takara) to generate S1972A and S1972D mutants. These vectors were transformed into BL21-DE3 Rosetta2 cells (Novagen) and expression of NS3h was induced with IPTG. Bacteria were pelleted and induction was verified by PAGE and One-Step Blue staining (Biotium). Bacteria were homogenized with a mechanical disruptor and lysate was purified over His-Pur Ni-NTA resin (Pierce). Peak fractions of protein eluate were pooled and dialyzed against storage buffer. Proteins were aliquoted and stored at −80° C. 1000ng of purified protein was run on a 10% Trisglycine gel and stained with One-Step Blue, and protein purity was determined by band densitometry using ImageJ.

***In vitro* ATPase assay:** *In vitro* assays were performed as previously described.[77] Briefly, 1.5mL of a reaction buffer containing 25mM MOPS pH 6.5, 5mg/mL BSA, 1.25mM $MgCl_2$, 0.01% Tween20, 10nM NS3h, 1.5μg/mL poly-U RNA (Sigma), and ATP from 10 to 300μM was assembled on ice. The tube was then incubated in a water bath at 37.0° C. 100μL fractions were transferred to a 96-well plate on ice containing 10μL 0.5M EDTA at 0, 10, 20, 30, 35, 40, 45, 50, 55, 60, 65, and 70 seconds. BioMol Green (Enzo) was added to quantify liberated phosphate. Phosphate accumulation curves were plotted and each curve

was used to determine the rate of ATP hydrolysis. Data were fit to a nonlinear regression using GraphPad Prism 10 to determine kinetic parameters of the purified NS3h proteins.

Kinase activity analysis: Kinase activity analysis was performed with the KSEA package in R (see data and code availability section for code access). KSEA was performed on phosphorylation sites ranked by Log2fold-change values using to the ProtMapper database of kinase-substrate interactions.[79,128] Only kinase-substrate interactions with a belief score of 1 were used for this analysis. Phosphorylation sites identified by peptides that were not unique to a single protein sequence and phosphorylation sites detected on multiply phosphorylated peptides were excluded from this analysis.

Kinase library analysis: Sequences surrounding each phosphorylation site within a range of +/− 7 amino acids were extracted using custom code in R (see data and code availability section for code access). These sequences were input into The Kinase Library enrichment analysis web tool.[78]

Viral life cycle assays

Entry: U2OS cells were transfected with siRNAs as previously described and allowed 48-72 hours to silence. Cells were infected with WNV NY2000 (MOI=10) for 120’ at 4° C, then shifted to 37° C for 0’ or 150’ to allow for internalization. After incubation at 37° C, cells were washed with ice-cold PBS and incubated with Proteinase K (1U/mL in DPBS supplemented with 3% heat-inactivated FBS) for 45’ at 4° C to remove virions bound to the cell surface, then washed three times with ice-cold PBS and collected in Trizol for quantitative RT-PCR.

Infection timecourse: U2OS cells were transfected with siRNAs as previously described and allowed 48-72 hours to silence. Cells were infected with WNV NY2000 (MOI=10) for 120’ at 4° C to synchronize infection, then moved to 37° C and collected in trizol at 0, 3, 6, 9, 12, 15, and 24 hours post-infection for quantitative RT-PCR.

Translation (WNV): HEK293T cells were transfected with siRNAs targeting PAK2 or a nontargeting control siRNA for 48 hours, then transfected with 400ng WNV replicon plasmid encoding *Renilla* luciferase with a catalytic mutation in NS5 (WNVII RepRenIB Pol^{-}) per well of 24-well plate.

Translation (DENV): DENV replicon RNA was produced by *in vitro* transcribing a linearized DENV replicon plasmid (Wild-type or Pol-dead)[108] using the T7 MEGAscript kit (Ambion). RNA was purified by LiCl precipitation and capped using the Vaccinia capping system (NEB) and stored at −80° C. HEK293T cells were silenced as described above and replated into 24-well plates after 48 hours. 24 hours after replating, cells were transfected with 1μg capped RNA using MessengerMax RNA transfection reagent per manufacturer instructions (Thermofisher). As a control, one pair of wells were treated with 25μg/mL cycloheximide preceding transfection and were collected at 4 hours post-transfection. Cells were collected at indicated timepoints in 0.1mL 1x passive lysis buffer and a *Renilla* luciferase assay was performed (Renilla-Glo, Promega).

Ongoing replication: Hek293T cells harboring a stably replicating WNV replicon were transfected with siRNAs as previously described and allowed 48-72 hours to silence. Cells were collected in Trizol and qRT-PCR performed on cDNA from transfected cells.

Multiple alignment analysis: The sequences of WNV NY99 proteins were aligned to those in closely related flaviviruses using the Clustal Omega Multiple Sequence Alignment tool (version 1.2.4) with default settings. Phosphorylated serine residues in NY99 proteins are denoted by red highlighting. Conservation of the post-translationally modified residues in related viruses is indicated by the same color scheme. Protein sequences were obtained from viral genome polyprotein sequences accessed on UniProt under the following reference numbers: WNV NY99, Q9Q6P4; WNV Kunjin, P14335; DENV-1, P17763; DENV-2, P14340; DENV-3, P27915; DENV-4, Q58HT7; ZIKV-FP A0A024B7W1; ZIKV-MR 766, Q32ZE1; JEV, P27395; YFV, Q6DV88.

Plasmids and generation of mutants: The NS2b/3 open reading frame from strain WNV NY 2000-crow 3356 was cloned into pCDNA4_TO with a C-terminal 2xStrep II affinity tag or a C-terminally 3X FLAG affinity tag for expression in human cells as previously described.[4] The lineage II WNV replicon encoding GFP or *Renilla* luciferase was a generous gift from Dr. Ted Pierson (NIH). The DENV replicons encoding *Renilla* luciferase were a generous gift from Jan Carette (Stanford). Mutations in each of the indicated sites were generated via site-directed mutagenesis using the In-Fusion HD Cloning Plus Kit (Takara). A complete list of primers used for cloning these constructs can be found in Table S10.

QUANTIFICATION AND STATISTICAL ANALYSIS

Statistical analyses were performed using R (proteomics, see STAR Methods) or Graphpad Prism. Details for specific experiments can be found in figure legends. Statistical tests include Student's T-test (unpaired) or one-way ANOVA with Bonferroni correction for multiple comparisons. For each experiment, n is indicated in the figure legend and is defined as one biological replicate. Data are presented as mean ± SD or SE as indicated in figure legends. Significance was defined as an adjusted p-value (corrected for multiple comparisons if necessary) of below 0.05.

ADDITIONAL RESOURCES

Raw data for proteomics and code for data analysis can be found at the PRIDE repository or Github (see key resources table for details).

Supplementary Material

Refer to Web version on PubMed Central for supplementary material.

ACKNOWLEDGMENTS

We thank members of the Cherry, Johnson, and Ramage labs for helpful discussions. We thank the University of Pennsylvania High-Throughput Screening Core for reagents and technical expertise. We thank Dr. Ted Pierson (WNV replicons encoding GFP and *Renilla* luciferase), Dr. Jan Carette (DENV replicons), and Dr. Russell Jones (*AMPK*α1/2$^{-/-}$ cells) for reagents. We thank Dr. Fabienne Paumet, Dr. Matthew Good, and Dr. Mikael Garabedian

for assistance with protein purification. We thank Dr. Jon Oakhill and Dr. Naomi Ling for their expertise on *AMPKβ1/2* function. This work was supported by NIH grant R01AI143850 to H.R.; NIH grants 1R01AI150246, R01AI152362, and R01AI140539 to S.C.; the Burroughs Wellcome Investigators in the Pathogenesis of Infectious Disease Award to S.C.; NIH grants R01AI124690 and R21AI187731 to J.R.J.; and NIH grant T32GM144302 supporting Z.W. and M.O. The graphical abstract was created using BioRender: Ramage, H. (2025) https://BioRender.com/2i452ni.

REFERENCES

1. Colpitts TM, Conway MJ, Montgomery RR, and Fikrig E (2012). West Nile Virus: biology, transmission, and human infection. Clin. Microbiol. Rev 25, 635–648. 10.1128/CMR.00045-12. [PubMed: 23034323]
2. Nash D, Mostashari F, Fine A, Miller J, O'Leary D, Murray K, Huang A, Rosenberg A, Greenberg A, Sherman M, et al. (2001). The outbreak of West Nile virus infection in the New York City area in 1999. N. Engl. J. Med 344, 1807–1814. 10.1056/NEJM200106143442401. [PubMed: 11407341]
3. Suthar MS, Diamond MS, and Gale M Jr. (2013). West Nile virus infection and immunity. Nat. Rev. Microbiol 11, 115–128. 10.1038/nrmicro2950. [PubMed: 23321534]
4. Li M, Johnson JR, Truong B, Kim G, Weinbren N, Dittmar M, Shah PS, Von Dollen J, Newton BW, Jang GM, et al. (2019). Identification of antiviral roles for the exon-junction complex and nonsense-mediated decay in flaviviral infection. Nat. Microbiol 4, 985–995. 10.1038/s41564-019-0375-z. [PubMed: 30833725]
5. Besson B, Basset J, Gatellier S, Chabrolles H, Chaze T, Hourdel V, Matondo M, Pardigon N, and Choumet V (2020). Comparison of a human neuronal model proteome upon Japanese encephalitis or West Nile Virus infection and potential role of mosquito saliva in neuropathogenesis. PLoS One 15, e0232585. 10.1371/journal.pone.0232585. [PubMed: 32374750]
6. Fraisier C, Camoin L, Lim SM, Bakli M, Belghazi M, Fourquet P, Granjeaud S, Osterhaus ADME, Koraka P, Martina B, and Almeras L (2013). Altered protein networks and cellular pathways in severe west nile disease in mice. PLoS One 8, e68318. 10.1371/journal.pone.0068318. [PubMed: 23874584]
7. Pastorino B, Boucomont-Chapeaublanc E, Peyrefitte CN, Belghazi M, Fusaï T, Rogier C, Tolou HJ, and Almeras L (2009). Identification of cellular proteome modifications in response to West Nile virus infection. Mol. Cell. Proteomics 8, 1623–1637. 10.1074/mcp.M800565-MCP200. [PubMed: 19395707]
8. Lee HJ, Zhao Y, Fleming I, Mehta S, Wang X, Wyk BV, Ronca SE, Kang H, Chou CH, Fatou B, et al. (2023). Early cellular and molecular signatures correlate with severity of West Nile virus infection. iScience 26, 108387. 10.1016/j.isci.2023.108387. [PubMed: 38047068]
9. Chiu HC, Hannemann H, Heesom KJ, Matthews DA, and Davidson AD (2014). High-throughput quantitative proteomic analysis of dengue virus type 2 infected A549 cells. PLoS One 9, e93305. 10.1371/journal.pone.0093305. [PubMed: 24671231]
10. Scaturro P, Stukalov A, Haas DA, Cortese M, Draganova K, Płaszczyca A, Bartenschlager R, Götz M, and Pichlmair A (2018). An orthogonal proteomic survey uncovers novel Zika virus host factors. Nature 561, 253–257. 10.1038/s41586-018-0484-5. [PubMed: 30177828]
11. Munro V, Kelly V, Messner CB, and Kustatscher G (2024). Cellular control of protein levels: A systems biology perspective. Proteomics 24, e2200220. 10.1002/pmic.202200220. [PubMed: 38012370]
12. Vogel C, and Marcotte EM (2012). Insights into the regulation of protein abundance from proteomic and transcriptomic analyses. Nat. Rev. Genet 13, 227–232. 10.1038/nrg3185. [PubMed: 22411467]
13. Zhao H, Chen M, Valdés A, Lind SB, and Pettersson U (2019). Transcriptomic and proteomic analyses reveal new insights into the regulation of immune pathways during adenovirus type 2 infection. BMC Microbiol. 19, 15. 10.1186/s12866-018-1375-5. [PubMed: 30642258]
14. Munoz-Jordan JL, and Fredericksen BL (2010). How flaviviruses activate and suppress the interferon response. Viruses 2, 676–691. 10.3390/v2020676. [PubMed: 21994652]
15. Suthar MS, Aguirre S, and Fernandez-Sesma A (2013). Innate immune sensing of flaviviruses. PLoS Pathog. 9, e1003541. 10.1371/journal.ppat.1003541. [PubMed: 24068919]

16. Slon Campos JL, Mongkolsapaya J, and Screaton GR (2018). The immune response against flaviviruses. Nat. Immunol 19, 1189–1198. 10.1038/s41590-018-0210-3. [PubMed: 30333606]

17. Roby JA, Setoh YX, Hall RA, and Khromykh AA (2015). Post-translational regulation and modifications of flavivirus structural proteins. J. Gen. Virol 96, 1551–1569. 10.1099/vir.0.000097. [PubMed: 25711963]

18. Serman T, Chiang C, Liu G, Sayyad Z, Pandey S, Volcic M, Lee H, Muppala S, Acharya D, Goins C, et al. (2023). Acetylation of the NS3 helicase by KAT5gamma is essential for flavivirus replication. Cell Host Microbe 31, 1317–1330.e1310. 10.1016/j.chom.2023.06.013. [PubMed: 37478852]

19. Hunziker A, Glas I, Pohl MO, and Stertz S (2022). Phosphoproteomic profiling of influenza virus entry reveals infection-triggered filopodia induction counteracted by dynamic cortactin phosphorylation. Cell Rep. 38, 110306. 10.1016/j.celrep.2022.110306. [PubMed: 35081340]

20. Bouhaddou M, Memon D, Meyer B, White KM, Rezelj VV, Correa Marrero M, Polacco BJ, Melnyk JE, Ulferts S, Kaake RM, et al. (2020). The Global Phosphorylation Landscape of SARS-CoV-2 Infection. Cell 182, 685–712.e19. 10.1016/j.cell.2020.06.034. [PubMed: 32645325]

21. Gracias S, Chazal M, Decombe A, Unterfinger Y, Sogues A, Pruvost L, Robert V, Lacour SA, Lemasson M, Sourisseau M, et al. (2023). Tick-borne flavivirus NS5 antagonizes interferon signaling by inhibiting the catalytic activity of TYK2. EMBO Rep. 24, e57424. 10.15252/embr.202357424. [PubMed: 37860832]

22. Lin YC, Jeng KS, and Lai MMC (2017). CNOT4-Mediated Ubiquitination of Influenza A Virus Nucleoprotein Promotes Viral RNA Replication. mBio 8, e00597–17. 10.1128/mBio.00597-17. [PubMed: 28536288]

23. Mondal A, Potts GK, Dawson AR, Coon JJ, and Mehle A (2015). Phosphorylation at the homotypic interface regulates nucleoprotein oligomerization and assembly of the influenza virus replication machinery. PLoS Pathog. 11, e1004826. 10.1371/journal.ppat.1004826. [PubMed: 25867750]

24. Zheng W, Li J, Wang S, Cao S, Jiang J, Chen C, Ding C, Qin C, Ye X, Gao GF, and Liu W (2015). Phosphorylation controls the nuclear-cytoplasmic shuttling of influenza A virus nucleoprotein. J. Virol 89, 5822–5834. 10.1128/JVI.00015-15. [PubMed: 25787277]

25. Fung TS, and Liu DX (2018). Post-translational modifications of coronavirus proteins: roles and function. Future Virol. 13, 405–430. 10.2217/fvl-2018-0008. [PubMed: 32201497]

26. Giraldo MI, Xia H, Aguilera-Aguirre L, Hage A, van Tol S, Shan C, Xie X, Sturdevant GL, Robertson SJ, McNally KL, et al. (2020). Envelope protein ubiquitination drives entry and pathogenesis of Zika virus. Nature 585, 414–419. 10.1038/s41586-020-2457-8. [PubMed: 32641828]

27. Mallagaray A, Creutznacher R, Dülfer J, Mayer PHO, Grimm LL, Orduñ a JM, Trabjerg E, Stehle T, Rand KD, Blaum BS, et al. (2019). A post-translational modification of human Norovirus capsid protein attenuates glycan binding. Nat. Commun 10, 1320. 10.1038/s41467-019-09251-5. [PubMed: 30899001]

28. Cheong YK, and Ng ML (2011). Dephosphorylation of West Nile virus capsid protein enhances the processes of nucleocapsid assembly. Microbes Infect. 13, 76–84. 10.1016/j.micinf.2010.10.014. [PubMed: 21034847]

29. Zhang J, Lan Y, Li MY, Lamers MM, Fusade-Boyer M, Klemm E, Thiele C, Ashour J, and Sanyal S (2018). Flaviviruses Exploit the Lipid Droplet Protein AUP1 to Trigger Lipophagy and Drive Virus Production. Cell Host Microbe 23, 819–831.e5. 10.1016/j.chom.2018.05.005. [PubMed: 29902443]

30. Mondal A, Dawson AR, Potts GK, Freiberger EC, Baker SF, Moser LA, Bernard KA, Coon JJ, and Mehle A (2017). Influenza virus recruits host protein kinase C to control assembly and activity of its replication machinery. Elife 6, e26910. 10.7554/eLife.26910. [PubMed: 28758638]

31. Johnson JR, Crosby DC, Hultquist JF, Kurland AP, Adhikary P, Li D, Marlett J, Swann J, Hüttenhain R, Verschueren E, et al. (2022). Global post-translational modification profiling of HIV-1-infected cells reveals mechanisms of host cellular pathway remodeling. Cell Rep. 39, 110690. 10.1016/j.celrep.2022.110690. [PubMed: 35417684]

32. Jones DM, Domingues P, Targett-Adams P, and McLauchlan J (2010). Comparison of U2OS and Huh-7 cells for identifying host factors that affect hepatitis C virus RNA replication. J. Gen. Virol 91, 2238–2248. 10.1099/vir.0.022210-0. [PubMed: 20505011]
33. Yasunaga A, Hanna SL, Li J, Cho H, Rose PP, Spiridigliozzi A, Gold B, Diamond MS, and Cherry S (2014). Genome-wide RNAi screen identifies broadly-acting host factors that inhibit arbovirus infection. PLoS Pathog. 10, e1003914. 10.1371/journal.ppat.1003914. [PubMed: 24550726]
34. Hackett BA, and Cherry S (2018). Flavivirus internalization is regulated by a size-dependent endocytic pathway. Proc. Natl. Acad. Sci. USA 115, 4246–4251. 10.1073/pnas.1720032115. [PubMed: 29610346]
35. Shah PS, Link N, Jang GM, Sharp PP, Zhu T, Swaney DL, Johnson JR, Von Dollen J, Ramage HR, Satkamp L, et al. (2018). Comparative Flavivirus-Host Protein Interaction Mapping Reveals Mechanisms of Dengue and Zika Virus Pathogenesis. Cell 175, 1931–1945.e18. 10.1016/j.cell.2018.11.028. [PubMed: 30550790]
36. Hackett BA, Dittmar M, Segrist E, Pittenger N, To J, Griesman T, Gordesky-Gold B, Schultz DC, and Cherry S (2019). Sirtuin Inhibitors Are Broadly Antiviral against Arboviruses. mBio 10, e01446–19. 10.1128/mBio.01446-19. [PubMed: 31289184]
37. Panda D, Rose PP, Hanna SL, Gold B, Hopkins KC, Lyde RB, Marks MS, and Cherry S (2013). Genome-wide RNAi screen identifies SEC61A and VCP as conserved regulators of Sindbis virus entry. Cell Rep. 5, 1737–1748. 10.1016/j.celrep.2013.11.028. [PubMed: 24332855]
38. Mertins P, Tang LC, Krug K, Clark DJ, Gritsenko MA, Chen L, Clauser KR, Clauss TR, Shah P, Gillette MA, et al. (2018). Reproducible workflow for multiplexed deep-scale proteome and phosphoproteome analysis of tumor tissues by liquid chromatography-mass spectrometry. Nat. Protoc 13, 1632–1661. 10.1038/s41596-018-0006-9. [PubMed: 29988108]
39. Xu G, Paige JS, and Jaffrey SR (2010). Global analysis of lysine ubiquitination by ubiquitin remnant immunoaffinity profiling. Nat. Biotechnol 28, 868–873. 10.1038/nbt.1654. [PubMed: 20639865]
40. Choi M, Chang CY, Clough T, Broudy D, Killeen T, MacLean B, and Vitek O (2014). MSstats: an R package for statistical analysis of quantitative mass spectrometry-based proteomic experiments. Bioinformatics 30, 2524–2526. 10.1093/bioinformatics/btu305. [PubMed: 24794931]
41. Afroz S, Giddaluru J, Abbas MM, and Khan N (2016). Transcriptome meta-analysis reveals a dysregulation in extra cellular matrix and cell junction associated gene signatures during Dengue virus infection. Sci. Rep 6, 33752. 10.1038/srep33752. [PubMed: 27651116]
42. Nakano A, Kato H, Watanabe T, Min KD, Yamazaki S, Asano Y, Seguchi O, Higo S, Shintani Y, Asanuma H, et al. (2010). AMPK controls the speed of microtubule polymerization and directional cell migration through CLIP-170 phosphorylation. Nat. Cell Biol 12, 583–590. 10.1038/ncb2060. [PubMed: 20495555]
43. Mustafa YM, Meuren LM, Coelho SVA, and de Arruda LB (2019). Pathways Exploited by Flaviviruses to Counteract the Blood-Brain Barrier and Invade the Central Nervous System. Front. Microbiol 10, 525. 10.3389/fmicb.2019.00525. [PubMed: 30984122]
44. Roe K, Kumar M, Lum S, Orillo B, Nerurkar VR, and Verma S (2012). West Nile virus-induced disruption of the blood-brain barrier in mice is characterized by the degradation of the junctional complex proteins and increase in multiple matrix metalloproteinases. J. Gen. Virol 93, 1193–1203. 10.1099/vir.0.040899-0. [PubMed: 22398316]
45. The Gene Ontology Consortium (2019). The Gene Ontology Resource: 20 years and still GOing strong. Nucleic Acids Res. 47, D330–D338. 10.1093/nar/gky1055. [PubMed: 30395331]
46. Schoggins JW, and Rice CM (2011). Interferon-stimulated genes and their antiviral effector functions. Curr. Opin. Virol 1, 519–525. 10.1016/j.coviro.2011.10.008. [PubMed: 22328912]
47. Schoggins JW, Wilson SJ, Panis M, Murphy MY, Jones CT, Bieniasz P, and Rice CM (2011). A diverse range of gene products are effectors of the type I interferon antiviral response. Nature 472, 481–485. 10.1038/nature09907. [PubMed: 21478870]
48. Rusinova I, Forster S, Yu S, Kannan A, Masse M, Cumming H, Chapman R, and Hertzog PJ (2013). Interferome v2.0: an updated database of annotated interferon-regulated genes. Nucleic Acids Res. 41, D1040–D1046. 10.1093/nar/gks1215. [PubMed: 23203888]

49. Blazquez AB, Escribano-Romero E, Merino-Ramos T, Saiz JC, and Martin-Acebes MA (2014). Stress responses in flavivirus-infected cells: activation of unfolded protein response and autophagy. Front. Microbiol 5, 266. 10.3389/fmicb.2014.00266. [PubMed: 24917859]
50. Ho DV, and Chan JY (2015). Induction of Herpud1 expression by ER stress is regulated by Nrf1. FEBS Lett. 589, 615–620. 10.1016/j.febslet.2015.01.026. [PubMed: 25637874]
51. Daffis S, Szretter KJ, Schriewer J, Li J, Youn S, Errett J, Lin TY, Schneller S, Zust R, Dong H, et al. (2010). 2'-O methylation of the viral mRNA cap evades host restriction by IFIT family members. Nature 468, 452–456. 10.1038/nature09489. [PubMed: 21085181]
52. Scherret JH, Poidinger M, Mackenzie JS, Broom AK, Deubel V, Lipkin WI, Briese T, Gould EA, and Hall RA (2001). The relationships between West Nile and Kunjin viruses. Emerg. Infect. Dis 7, 697–705. 10.3201/eid0704.010418. [PubMed: 11585535]
53. Diamond MS (2014). IFIT1: A dual sensor and effector molecule that detects non-2'-O methylated viral RNA and inhibits its translation. Cytokine Growth Factor Rev. 25, 543–550. 10.1016/j.cytogfr.2014.05.002. [PubMed: 24909568]
54. Diamond MS, and Farzan M (2013). The broad-spectrum antiviral functions of IFIT and IFITM proteins. Nat. Rev. Immunol 13, 46–57. 10.1038/nri3344. [PubMed: 23237964]
55. Pichlmair A, Lassnig C, Eberle CA, Górna MW, Baumann CL, Burkard TR, Bürckstü mmer T, Stefanovic A, Krieger S, Bennett KL, et al. (2011). IFIT1 is an antiviral protein that recognizes 5'-triphosphate RNA. Nat. Immunol 12, 624–630. 10.1038/ni.2048. [PubMed: 21642987]
56. Johnson B, VanBlargan LA, Xu W, White JP, Shan C, Shi PY, Zhang R, Adhikari J, Gross ML, Leung DW, et al. (2018). Human IFIT3 Modulates IFIT1 RNA Binding Specificity and Protein Stability. Immunity 48, 487–499.e5. 10.1016/j.immuni.2018.01.014. [PubMed: 29525521]
57. Leto DE, Morgens DW, Zhang L, Walczak CP, Elias JE, Bassik MC, and Kopito RR (2019). Genome-wide CRISPR Analysis Identifies Substrate-Specific Conjugation Modules in ER-Associated Degradation. Mol. Cell 73, 377–389.e11. 10.1016/j.molcel.2018.11.015. [PubMed: 30581143]
58. Kokame K, Agarwala KL, Kato H, and Miyata T (2000). Herp, a new ubiquitin-like membrane protein induced by endoplasmic reticulum stress. J. Biol. Chem 275, 32846–32853. 10.1074/jbc.M002063200. [PubMed: 10922362]
59. Okuda-Shimizu Y, and Hendershot LM (2007). Characterization of an ERAD pathway for nonglycosylated BiP substrates, which require Herp. Mol. Cell 28, 544–554. 10.1016/j.molcel.2007.09.012. [PubMed: 18042451]
60. Krishnan MN, Ng A, Sukumaran B, Gilfoy FD, Uchil PD, Sultana H, Brass AL, Adametz R, Tsui M, Qian F, et al. (2008). RNA interference screen for human genes associated with West Nile virus infection. Nature 455, 242–245. 10.1038/nature07207. [PubMed: 18690214]
61. Zhang R, Miner JJ, Gorman MJ, Rausch K, Ramage H, White JP, Zuiani A, Zhang P, Fernandez E, Zhang Q, et al. (2016). A CRISPR screen defines a signal peptide processing pathway required by flaviviruses. Nature 535, 164–168. 10.1038/nature18625. [PubMed: 27383988]
62. Anton A, Mazeaud C, Freppel W, Gilbert C, Tremblay N, Sow AA, Roy M, Rodrigue-Gervais IG, and Chatel-Chaix L (2021). Valosin-containing protein ATPase activity regulates the morphogenesis of Zika virus replication organelles and virus-induced cell death. Cell. Microbiol 23, e13302. 10.1111/cmi.13302. [PubMed: 33432690]
63. Sehrawat S, Khasa R, Deb A, Prajapat SK, Mallick S, Basu A, Surjit M, Kalia M, and Vrati S (2021). Valosin-containing protein/p97 plays critical roles in the Japanese encephalitis virus life cycle. J. Virol 95, e02336–20. 10.1128/JVI.02336-20. [PubMed: 33731458]
64. Tabata K, Arakawa M, Ishida K, Kobayashi M, Nara A, Sugimoto T, Okada T, Mori K, and Morita E (2021). Endoplasmic Reticulum-Associated Degradation Controls Virus Protein Homeostasis, Which Is Required for Flavivirus Propagation. J. Virol 95, e0223420. 10.1128/JVI.02234-20. [PubMed: 33980593]
65. Huang CH, Chu YR, Ye Y, and Chen X (2014). Role of HERP and a HERP-related protein in HRD1-dependent protein degradation at the endoplasmic reticulum. J. Biol. Chem 289, 4444–4454. 10.1074/jbc.M113.519561. [PubMed: 24366871]

66. Ballar P, Pabuccuoglu A, and Kose FA (2011). Different p97/VCP complexes function in retrotranslocation step of mammalian ER-associated degradation (ERAD). Int. J. Biochem. Cell Biol 43, 613–621. 10.1016/j.biocel.2010.12.021. [PubMed: 21199683]

67. Sugimoto T, Ninagawa S, Yamano S, Ishikawa T, Okada T, Takeda S, and Mori K (2017). SEL1L-dependent Substrates Require Derlin2/3 and Herp1/2 for Endoplasmic Reticulum-associated Degradation. Cell Struct. Funct 42, 81–94. 10.1247/csf.17007. [PubMed: 28552883]

68. Bhuvanakantham R, Cheong YK, and Ng ML (2010). West Nile virus capsid protein interaction with importin and HDM2 protein is regulated by protein kinase C-mediated phosphorylation. Microbes Infect. 12, 615–625. 10.1016/j.micinf.2010.04.005. [PubMed: 20417716]

69. Keating JA, Bhattacharya D, Lim PY, Falk S, Weisblum B, Bernard KA, Sharma M, Kuhn RJ, and Striker R (2013). West Nile virus methyltransferase domain interacts with protein kinase G. Virol. J 10, 242. 10.1186/1743-422X-10-242. [PubMed: 23876037]

70. Dong H, Zhang B, and Shi PY (2008). Flavivirus methyltransferase: a novel antiviral target. Antiviral Res. 80, 1–10. 10.1016/j.antiviral.2008.05.003. [PubMed: 18571739]

71. Pierson TC, Sánchez MD, Puffer BA, Ahmed AA, Geiss BJ, Valentine LE, Altamura LA, Diamond MS, and Doms RW (2006). A rapid and quantitative assay for measuring antibody-mediated neutralization of West Nile virus infection. Virology 346, 53–65. 10.1016/j.virol.2005.10.030. [PubMed: 16325883]

72. Lopez-Denman AJ, Russo A, Wagstaff KM, White PA, Jans DA, and Mackenzie JM (2018). Nucleocytoplasmic shuttling of the West Nile virus RNA-dependent RNA polymerase NS5 is critical to infection. Cell. Microbiol 20, e12848. 10.1111/cmi.12848. [PubMed: 29582535]

73. Tay MYF, Smith K, Ng IHW, Chan KWK, Zhao Y, Ooi EE, Lescar J, Luo D, Jans DA, Forwood JK, and Vasudevan SG (2016). The C-terminal 18 Amino Acid Region of Dengue Virus NS5 Regulates its Subcellular Localization and Contains a Conserved Arginine Residue Essential for Infectious Virus Production. PLoS Pathog. 12, e1005886. 10.1371/journal.ppat.1005886. [PubMed: 27622521]

74. Mastrangelo E, Milani M, Bollati M, Selisko B, Peyrane F, Pandini V, Sorrentino G, Canard B, Konarev PV, Svergun DI, et al. (2007). Crystal structure and activity of Kunjin virus NS3 helicase; protease and helicase domain assembly in the full length NS3 protein. J. Mol. Biol 372, 444–455. 10.1016/j.jmb.2007.06.055. [PubMed: 17658551]

75. Du Pont KE, Davidson RB, McCullagh M, and Geiss BJ (2020). Motif V regulates energy transduction between the flavivirus NS3 ATPase and RNA-binding cleft. J. Biol. Chem 295, 1551–1564. 10.1074/jbc.RA119.011922. [PubMed: 31914411]

76. Du Pont KE, McCullagh M, and Geiss BJ (2022). Conserved motifs in the flavivirus NS3 RNA helicase enzyme. Wiley Interdiscip. Rev. RNA 13, e1688. 10.1002/wrna.1688. [PubMed: 34472205]

77. Roy P, Walter Z, Berish L, Ramage H, and McCullagh M (2024). Motif-VI loop acts as a nucleotide valve in the West Nile Virus NS3 Helicase. Nucleic Acids Res. 52, 7447–7464. 10.1093/nar/gkae500. [PubMed: 38884215]

78. Johnson JL, Yaron TM, Huntsman EM, Kerelsky A, Song J, Regev A, Lin TY, Liberatore K, Cizin DM, Cohen BM, et al. (2023). An atlas of substrate specificities for the human serine/threonine kinome. Nature 613, 759–766. 10.1038/s41586-022-05575-3. [PubMed: 36631611]

79. Hernandez-Armenta C, Ochoa D, Gonçalves E, Saez-Rodriguez J, and Beltrao P (2017). Benchmarking substrate-based kinase activity inference using phosphoproteomic data. Bioinformatics 33, 1845–1851. 10.1093/bioinformatics/btx082. [PubMed: 28200105]

80. Hornbeck PV, Zhang B, Murray B, Kornhauser JM, Latham V, and Skrzypek E (2015). PhosphoSitePlus, 2014: mutations, PTMs and recalibrations. Nucleic Acids Res. 43, D512–D520. 10.1093/nar/gku1267. [PubMed: 25514926]

81. Alzhanova D, Corcoran K, Bailey AG, Long K, Taft-Benz S, Graham RL, Broussard GS, Heise M, Neumann G, Halfmann P, et al. (2021). Novel modulators of p53-signaling encoded by unknown genes of emerging viruses. PLoS Pathog. 17, e1009033. 10.1371/journal.ppat.1009033. [PubMed: 33411764]

82. Gehring T, Seeholzer T, and Krappmann D (2018). BCL10 - Bridging CARDs to Immune Activation. Front. Immunol 9, 1539. 10.3389/fimmu.2018.01539. [PubMed: 30022982]

83. Ma-Lauer Y, Carbajo-Lozoya J, Hein MY, Müller MA, Deng W, Lei J, Meyer B, Kusov Y, von Brunn B, Bairad DR, et al. (2016). p53 down-regulates SARS coronavirus replication and is targeted by the SARS-unique domain and PLpro via E3 ubiquitin ligase RCHY1. Proc. Natl. Acad. Sci. USA 113, E5192–E5201. 10.1073/pnas.1603435113. [PubMed: 27519799]
84. Rivas C, Aaronson SA, and Munoz-Fontela C (2010). Dual Role of p53 in Innate Antiviral Immunity. Viruses 2, 298–313. 10.3390/v2010298. [PubMed: 21994612]
85. Yang D, Pei G, Dong S, Zhang W, Deng H, Zhao X, Li P, and Lin X (2023). Bcl10 phosphorylation-dependent droplet-like condensation positively regulates DNA virus-induced innate immune signaling. Sci. China Life Sci 66, 283–297. 10.1007/s11427-022-2169-x. [PubMed: 36115893]
86. Gonzalez A, Hall MN, Lin SC, and Hardie DG (2020). AMPK and TOR: The Yin and Yang of Cellular Nutrient Sensing and Growth Control. Cell Metab. 31, 472–492. 10.1016/j.cmet.2020.01.015. [PubMed: 32130880]
87. Moser TS, Schieffer D, and Cherry S (2012). AMP-activated kinase restricts Rift Valley fever virus infection by inhibiting fatty acid synthesis. PLoS Pathog. 8, e1002661. 10.1371/journal.ppat.1002661. [PubMed: 22532801]
88. Willows R, Sanders MJ, Xiao B, Patel BR, Martin SR, Read J, Wilson JR, Hubbard J, Gamblin SJ, and Carling D (2017). Phosphorylation of AMPK by upstream kinases is required for activity in mammalian cells. Biochem. J 474, 3059–3073. 10.1042/BCJ20170458. [PubMed: 28694351]
89. Singh S, Singh PK, Suhail H, Arumugaswami V, Pellett PE, Giri S, and Kumar A (2020). AMP-Activated Protein Kinase Restricts Zika Virus Replication in Endothelial Cells by Potentiating Innate Antiviral Responses and Inhibiting Glycolysis. J. Immunol 204, 1810–1824. 10.4049/jimmunol.1901310. [PubMed: 32086387]
90. Thaker SK, Chapa T, Garcia G Jr., Gong D, Schmid EW, Arumugaswami V, Sun R, and Christofk HR (2019). Differential Metabolic Reprogramming by Zika Virus Promotes Cell Death in Human versus Mosquito Cells. Cell Metab. 29, 1206–1216.e4. 10.1016/j.cmet.2019.01.024. [PubMed: 30827860]
91. Warden SM, Richardson C, O'Donnell J Jr., Stapleton D, Kemp BE, and Witters LA (2001). Post-translational modifications of the beta-1 subunit of AMP-activated protein kinase affect enzyme activity and cellular localization. Biochem. J 354, 275–283. 10.1042/0264-6021:3540275. [PubMed: 11171104]
92. Desjardins EM, Smith BK, Day EA, Ducommun S, Sanders MJ, Nederveen JP, Ford RJ, Pinkosky SL, Townsend LK, Gutgesell RM, et al. (2022). The phosphorylation of AMPKbeta1 is critical for increasing autophagy and maintaining mitochondrial homeostasis in response to fatty acids. Proc. Natl. Acad. Sci. USA 119, e2119824119. 10.1073/pnas.2119824119. [PubMed: 36409897]
93. Dite TA, Ling NXY, Scott JW, Hoque A, Galic S, Parker BL, Ngoei KRW, Langendorf CG, O'Brien MT, Kundu M, et al. (2017). The autophagy initiator ULK1 sensitizes AMPK to allosteric drugs. Nat. Commun 8, 571. 10.1038/s41467-017-00628-y. [PubMed: 28924239]
94. Sanders MJ, Ali ZS, Hegarty BD, Heath R, Snowden MA, and Carling D (2007). Defining the mechanism of activation of AMP-activated protein kinase by the small molecule A-769662, a member of the thienopyridone family. J. Biol. Chem 282, 32539–32548. 10.1074/jbc.M706543200. [PubMed: 17728241]
95. Jimenez de Oya N, Blazquez AB, Casas J, Saiz JC, and Martin-Acebes MA (2018). Direct Activation of Adenosine Monophosphate-Activated Protein Kinase (AMPK) by PF-06409577 Inhibits Flavivirus Infection through Modification of Host Cell Lipid Metabolism. Antimicrob. Agents Chemother 62, e00360–18. 10.1128/AAC.00360-18. [PubMed: 29712653]
96. Jordan TX, and Randall G (2017). Dengue Virus Activates the AMP Kinase-mTOR Axis To Stimulate a Proviral Lipophagy. J. Virol 91, e02020–16. 10.1128/JVI.02020-16. [PubMed: 28298606]
97. Soto-Acosta R, Bautista-Carbajal P, Cervantes-Salazar M, Angel-Ambrocio AH, and Del Angel RM (2017). DENV up-regulates the HMG-CoA reductase activity through the impairment of AMPK phosphorylation: A potential antiviral target. PLoS Pathog. 13, e1006257. 10.1371/journal.ppat.1006257. [PubMed: 28384260]
98. Winkelmann ER, Luo H, and Wang T (2016). West Nile Virus Infection in the Central Nervous SystemF1000 Faculty Rev-105. F1000Res. 5. 10.12688/f1000research.7404.1.

99. Munday MR (2002). Regulation of mammalian acetyl-CoA carboxylase. Biochem. Soc. Trans 30, 1059–1064. 10.1042/bst0301059. [PubMed: 12440972]

100. Jimenez de Oya N, Esler WP, Huard K, El-Kattan AF, Karamanlidis G, Blazquez AB, Ramos-Ibeas P, Escribano-Romero E, Louloudes-Lazaro A, Casas J, et al. (2019). Targeting host metabolism by inhibition of acetyl-Coenzyme A carboxylase reduces flavivirus infection in mouse models. Emerg Microbes Infect 8, 624–636. 10.1080/22221751.2019.1604084. [PubMed: 30999821]

101. Wu W, Chen R, Wan Y, Li L, Han J, Lei Q, Chen Z, Liu S, and Yao X (2022). Acetyl-CoA Carboxylase (ACC) Inhibitor, CP640186, Effectively Inhibited Dengue Virus (DENV) Infection via Regulating ACC Phosphorylation. Molecules 27, 8583. 10.3390/molecules27238583. [PubMed: 36500675]

102. Zhang Q, Liu S, Zhang CS, Wu Q, Yu X, Zhou R, Meng F, Wang A, Zhang F, Chen S, et al. (2022). AMPK directly phosphorylates TBK1 to integrate glucose sensing into innate immunity. Mol. Cell 82, 4519–4536.e7. 10.1016/j.molcel.2022.10.026. [PubMed: 36384137]

103. Jung JH, and Traugh JA (2005). Regulation of the interaction of Pak2 with Cdc42 via autophosphorylation of serine 141. J. Biol. Chem 280, 40025–40031. 10.1074/jbc.M509075200. [PubMed: 16204230]

104. Gatti A, Huang Z, Tuazon PT, and Traugh JA (1999). Multisite autophosphorylation of p21-activated protein kinase gamma-PAK as a function of activation. J. Biol. Chem 274, 8022–8028. 10.1074/jbc.274.12.8022. [PubMed: 10075701]

105. Van den Broeke C, Radu M, Deruelle M, Nauwynck H, Hofmann C, Jaffer ZM, Chernoff J, and Favoreel HW (2009). Alphaherpesvirus US3-mediated reorganization of the actin cytoskeleton is mediated by group A p21-activated kinases. Proc. Natl. Acad. Sci. USA 106, 8707–8712. 10.1073/pnas.0900436106. [PubMed: 19435845]

106. Zhang Y, Gao W, Li J, Wu W, and Jiu Y (2019). The Role of Host Cytoskeleton in Flavivirus Infection. Virol. Sin 34, 30–41. 10.1007/s12250-019-00086-4. [PubMed: 30725318]

107. Ling J, Morley SJ, and Traugh JA (2005). Inhibition of cap-dependent translation via phosphorylation of eIF4G by protein kinase Pak2. EMBO J. 24, 4094–4105. 10.1038/sj.emboj.7600868. [PubMed: 16281055]

108. Marceau CD, Puschnik AS, Majzoub K, Ooi YS, Brewer SM, Fuchs G, Swaminathan K, Mata MA, Elias JE, Sarnow P, and Carette JE (2016). Genetic dissection of Flaviviridae host factors through genome-scale CRISPR screens. Nature 535, 159–163. 10.1038/nature18631. [PubMed: 27383987]

109. Otto GA, and Puglisi JD (2004). The pathway of HCV IRES-mediated translation initiation. Cell 119, 369–380. 10.1016/j.cell.2004.09.038. [PubMed: 15507208]

110. McDougal MB, De Maria AM, Ohlson MB, Kumar A, Xing C, and Schoggins JW (2023). Interferon inhibits a model RNA virus via a limited set of inducible effector genes. EMBO Rep. 24, e56901. 10.15252/embr.202356901. [PubMed: 37497756]

111. Leitman J, Shenkman M, Gofman Y, Shtern NO, Ben-Tal N, Hendershot LM, and Lederkremer GZ (2014). Herp coordinates compartmentalization and recruitment of HRD1 and misfolded proteins for ERAD. Mol. Biol. Cell 25, 1050–1060. 10.1091/mbc.E13-06-0350. [PubMed: 24478453]

112. Lemay KL, Treadaway J, Angulo I, and Tellinghuisen TL (2013). A hepatitis C virus NS5A phosphorylation site that regulates RNA replication. J. Virol 87, 1255–1260. 10.1128/JVI.02154-12. [PubMed: 23115292]

113. Yamauchi S, Takeuchi K, Chihara K, Sun X, Honjoh C, Yoshiki H, Hotta H, and Sada K (2015). Hepatitis C Virus Particle Assembly Involves Phosphorylation of NS5A by the c-Abl Tyrosine Kinase. J. Biol. Chem 290, 21857–21864. 10.1074/jbc.M115.666859. [PubMed: 26203192]

114. Zhu Z, Chu H, Wen L, Yuan S, Chik KKH, Yuen TTT, Yip CCY, Wang D, Zhou J, Yin F, et al. (2019). Targeting SUMO Modification of the Non-Structural Protein 5 of Zika Virus as a Host-Targeting Antiviral Strategy. Int. J. Mol. Sci 20, 392. 10.3390/ijms20020392. [PubMed: 30658479]

115. Giraldo MI, Vargas-Cuartas O, Gallego-Gomez JC, Shi PY, Padilla-Sanabria L, Castaño-Osorio JC, and Rajsbaum R (2018). K48-linked polyubiquitination of dengue virus NS1 protein inhibits

its interaction with the viral partner NS4B. Virus Res. 246, 1–11. 10.1016/j.virusres.2017.12.013. [PubMed: 29294313]

116. Ross-Thriepland D, Mankouri J, and Harris M (2015). Serine phosphorylation of the hepatitis C virus NS5A protein controls the establishment of replication complexes. J. Virol 89, 3123–3135. 10.1128/JVI.02995-14. [PubMed: 25552726]
117. Swarbrick CMD, Basavannacharya C, Chan KWK, Chan SA, Singh D, Wei N, Phoo WW, Luo D, Lescar J, and Vasudevan SG (2017). NS3 helicase from dengue virus specifically recognizes viral RNA sequence to ensure optimal replication. Nucleic Acids Res. 45, 12904–12920. 10.1093/nar/gkx1127. [PubMed: 29165589]
118. Garcia D, and Shaw RJ (2017). AMPK: Mechanisms of Cellular Energy Sensing and Restoration of Metabolic Balance. Mol. Cell 66, 789–800. 10.1016/j.molcel.2017.05.032. [PubMed: 28622524]
119. Prantner D, Perkins DJ, and Vogel SN (2017). AMP-activated Kinase (AMPK) Promotes Innate Immunity and Antiviral Defense through Modulation of Stimulator of Interferon Genes (STING) Signaling. J. Biol. Chem 292, 292–304. 10.1074/jbc.M116.763268. [PubMed: 27879319]
120. Pascua PNQ, Lee JH, Song MS, Park SJ, Baek YH, Ann BH, Shin EY, Kim EG, and Choi YK (2011). Role of the p21-activated kinases (PAKs) in influenza A virus replication. Biochem. Biophys. Res. Commun 414, 569–574. 10.1016/j.bbrc.2011.09.119. [PubMed: 21982772]
121. Van den Broeke C, Radu M, Chernoff J, and Favoreel HW (2010). An emerging role for p21-activated kinases (Paks) in viral infections. Trends Cell Biol. 20, 160–169. 10.1016/j.tcb.2009.12.005. [PubMed: 20071173]
122. Perez-Riverol Y, Bai J, Bandla C, García-Seisdedos D, Hewapathirana S, Kamatchinathan S, Kundu DJ, Prakash A, Frericks-Zipper A, Eisenacher M, et al. (2022). The PRIDE database resources in 2022: a hub for mass spectrometry-based proteomics evidences. Nucleic Acids Res. 50, D543–D552. 10.1093/nar/gkab1038. [PubMed: 34723319]
123. Rausch K, Hackett BA, Weinbren NL, Reeder SM, Sadovsky Y, Hunter CA, Schultz DC, Coyne CB, and Cherry S (2017). Screening Bioactives Reveals Nanchangmycin as a Broad Spectrum Antiviral Active against Zika Virus. Cell Rep. 18, 804–815. 10.1016/j.celrep.2016.12.068. [PubMed: 28099856]
124. Cox J, and Mann M (2008). MaxQuant enables high peptide identification rates, individualized p.p.b.-range mass accuracies and proteome-wide protein quantification. Nat. Biotechnol 26, 1367–1372. 10.1038/nbt.1511. [PubMed: 19029910]
125. Ashburner M, Ball CA, Blake JA, Botstein D, Butler H, Cherry JM, Davis AP, Dolinski K, Dwight SS, Eppig JT, et al. (2000). Gene ontology: tool for the unification of biology. The Gene Ontology Consortium. Nat. Genet 25, 25–29. 10.1038/75556. [PubMed: 10802651]
126. Gene Ontology Consortium (2021). The Gene Ontology resource: enriching a GOld mine. Nucleic Acids Res. 49, D325–D334. 10.1093/nar/gkaa1113. [PubMed: 33290552]
127. Birmingham A, Selfors LM, Forster T, Wrobel D, Kennedy CJ, Shanks E, Santoyo-Lopez J, Dunican DJ, Long A, Kelleher D, et al. (2009). Statistical methods for analysis of high-throughput RNA interference screens. Nat. Methods 6, 569–575. 10.1038/nmeth.1351. [PubMed: 19644458]
128. Bachman JA, Sorger PK, and Gyori BM (2022). Assembling a corpus of phosphoproteomic annotations using ProtMapper to normalize site information from databases and text mining. Preprint at bioRxiv. 10.1101/822668.

Highlights

- Protein abundance changes in infected cells are regulated post-transcriptionally
- Phosphorylation of viral non-structural proteins influences viral RNA replication
- Kinases AMPK and PAK2 are activated by phosphorylation during viral infection
- PAK2 limits West Nile virus replication by inhibiting viral genome translation

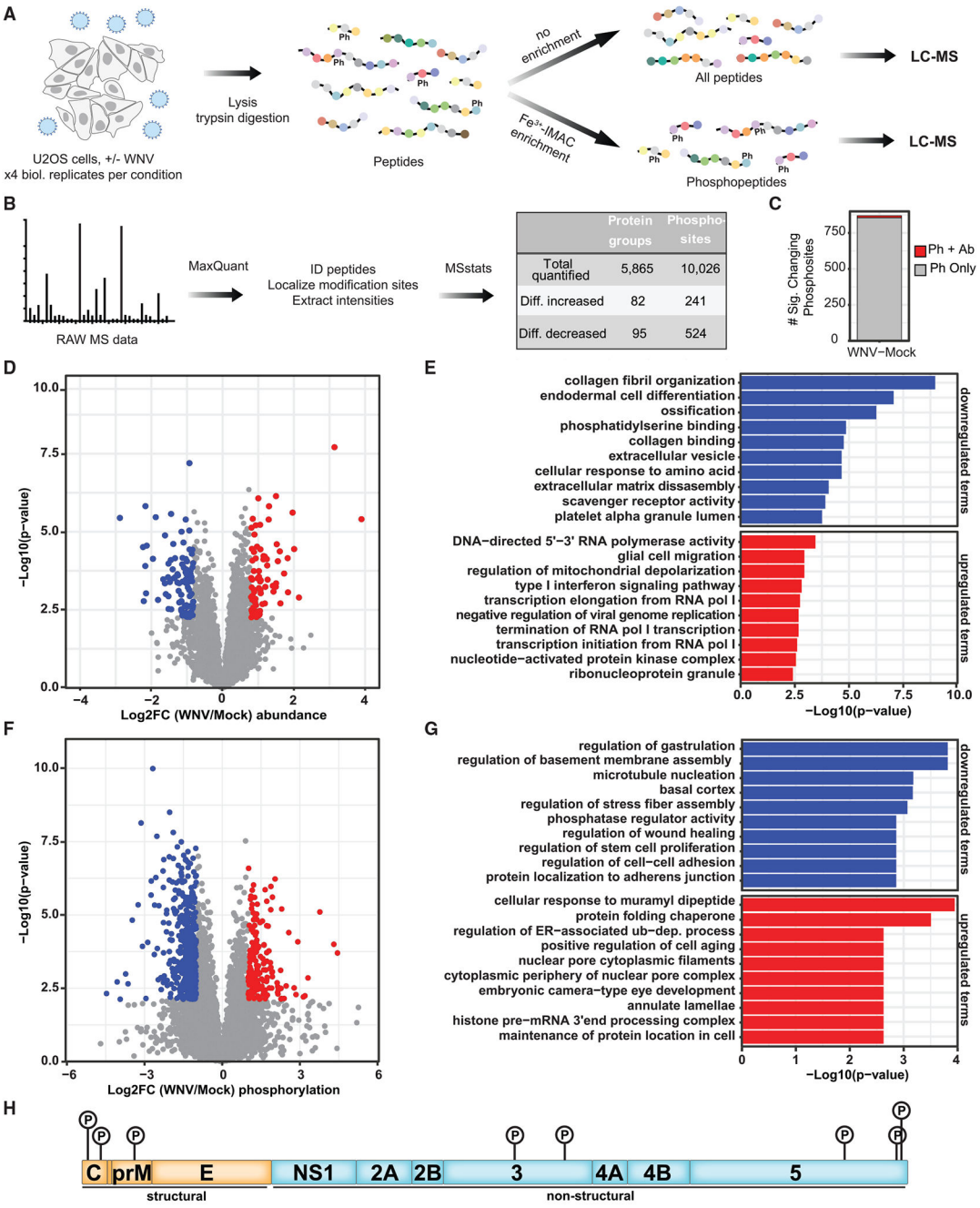

Figure 1. Quantification of protein changes during WNV infection

(A and B) Strategy to generate proteomic samples (A) and quantify changes in protein abundance and phosphorylation (B).

(C) Proteins with significant phosphosites and abundance changes (red) vs. proteins with only significant changes in phosphosites (gray).

(D) Volcano plot depicting upregulated (red) or downregulated (blue) peptides. Shown is log2 fold change of protein abundance (*x* axis) vs. −log10 adjusted *p* value (*y* axis).

(E) Enriched terms for proteins with increased (red) or decreased abundance (blue) upon WNV infection. The magnitude represents statistical significance (−log(*p* value)).

(F) Volcano plot depicting protein phosphorylation changes as in (D).

(G) Enriched terms for increased or decreased phosphorylation as in (E).

(H) WNV polyprotein with indicated phosphorylated residues.

For all MS data, $n = 4$. See also Figures S1 and S2; Tables S1, S2, S3, and S4; and Data S1.

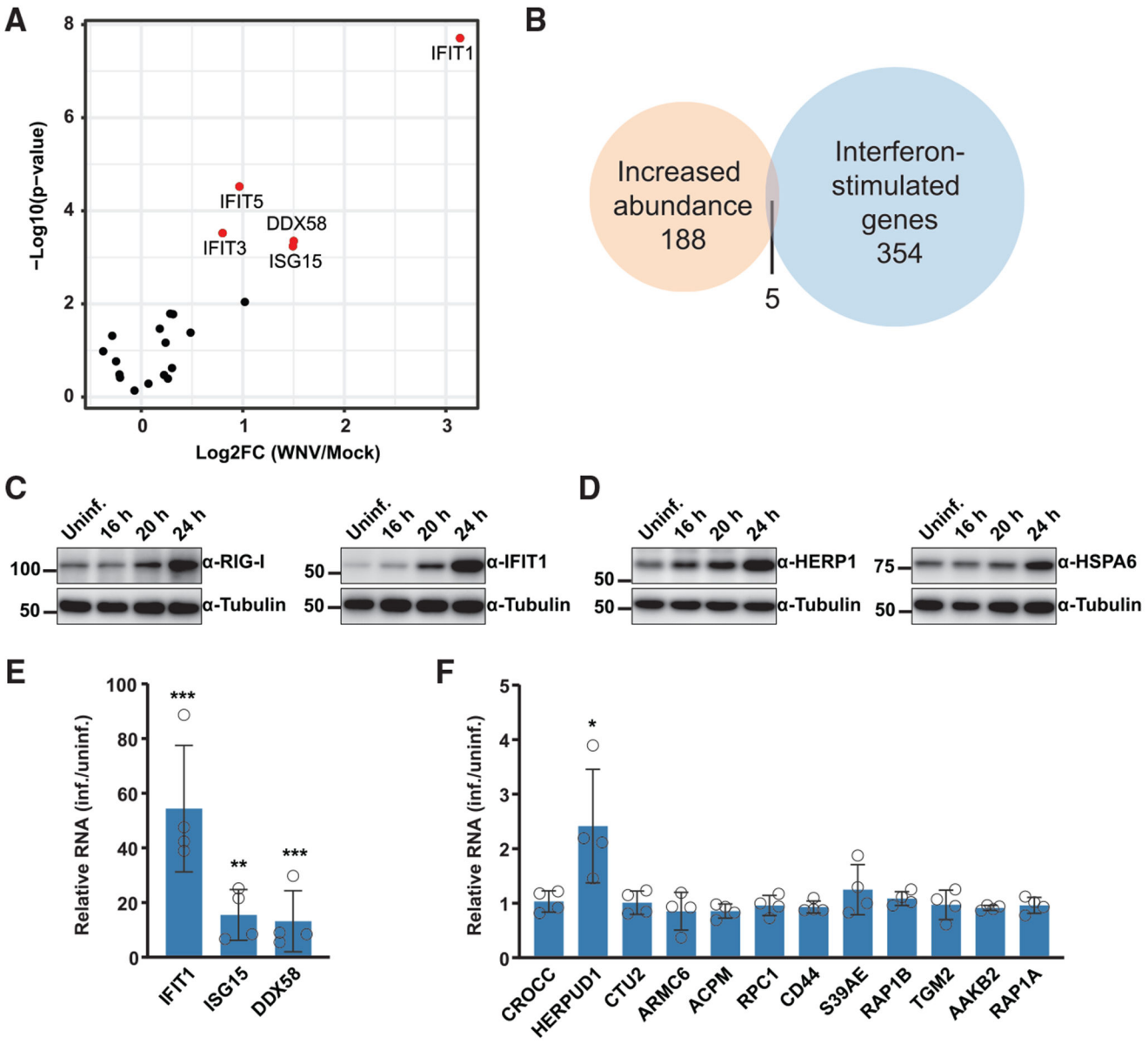

Figure 2. Protein abundance changes during WNV infection

(A) Volcano plot showing expression of known antiviral ISGs.

(B) Overlap of proteins with increased abundance with known antiviral ISGs.

(C and D) U2OS cells were infected with WNV NY2000 (MOI 1) and lysates were probed with the indicated antibodies.

(E) Relative RNA of indicated ISGs with increased protein abundance from WNV-infected cells.

(F) Relative RNA of indicated transcripts with increased protein abundance from WNV-infected cells.

For all data, the mean ± SD is shown; $n = 4$. Western blot data are representative of ≥2 independent experiments. Significance is indicated by $*p < 0.05$, $**p < 0.005$, or $***p < 0.0005$; two-tailed Student's t test. See also Table S5.

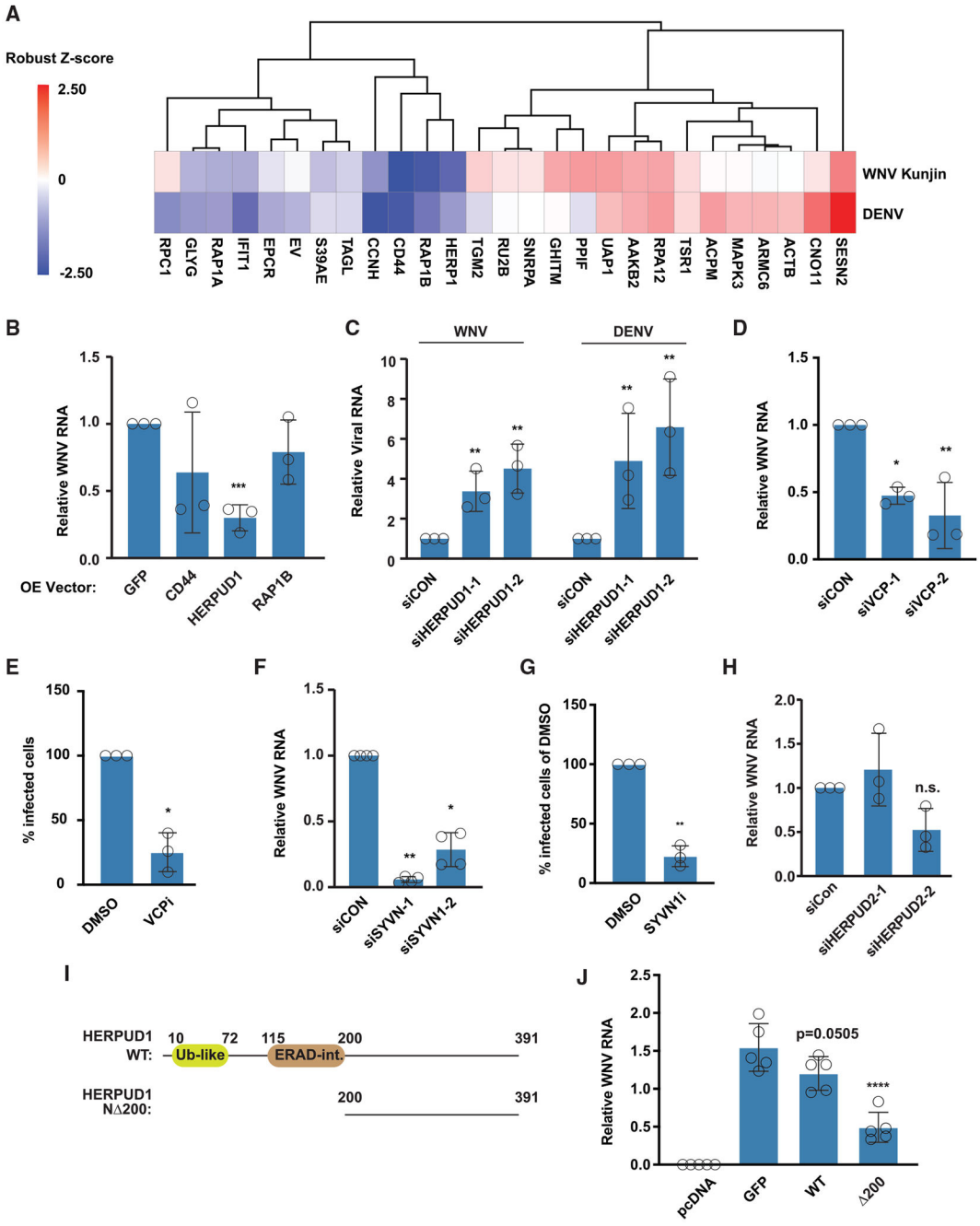

Figure 3. Overexpression screen for upregulated proteins

(A) Heatmap of average robust *Z* scores for WNV Kunjin or DENV infection upon cDNA overexpression ($n = 2$; Table S6) with rows clustered by Euclidean distance.

(B) Relative RNA of WNV NY2000 in HEK293T cells transfected with cDNA constructs, normalized to a control GFP-expressing vector. $n = 3$.

(C) Relative WNV NY2000 or DENV viral RNA upon HERPUD1 silencing, normalized to siControl (siCON). $n = 3$.

(D) Relative WNV RNA in U2OS cells transfected with control or VCP siRNAs, normalized as in (C). $n = 3$.

(E) Cells were treated with VCP inhibitor Eey1 (VCPi; 5 μM) or DMSO and infected with WNV Kunjin for 24 h. Infection was quantified using immunofluorescence microscopy and normalized to DMSO control. $n = 3$.

(F) Relative viral RNA following infection with WNV NY2000 upon silencing of SYVN1, normalized as in (C). $n = 4$.

(G) Relative percentage infection of WNV Kunjin in cells treated with an SYVN1 inhibitor (LS102, 10 μM) or DMSO. Shown is the DMSO-normalized percentage infection. $n = 3$.

(H) Relative viral RNA following infection with WNV NY2000 upon HERPUD2 knockdown. Infections are normalized as in (C). $n = 3$.

(I) The ubiquitin-like (Ub-like) and the ERAD protein (UBQLN1 and SYVN1)-interacting (ERAD-int.) domains of HERPUD1.

(J) Relative WNV replicon RNA from cells co-transfected with the indicated vectors. $n = 5$.

For all data, the mean ± SD is shown. Significance is indicated by $*p < 0.05$, $**p < 0.005$, or $***p < 0.0005$; two-tailed Student's t test or Welch's ANOVA with Bonferroni *post hoc* correction. See also Figure S3; Table S6.

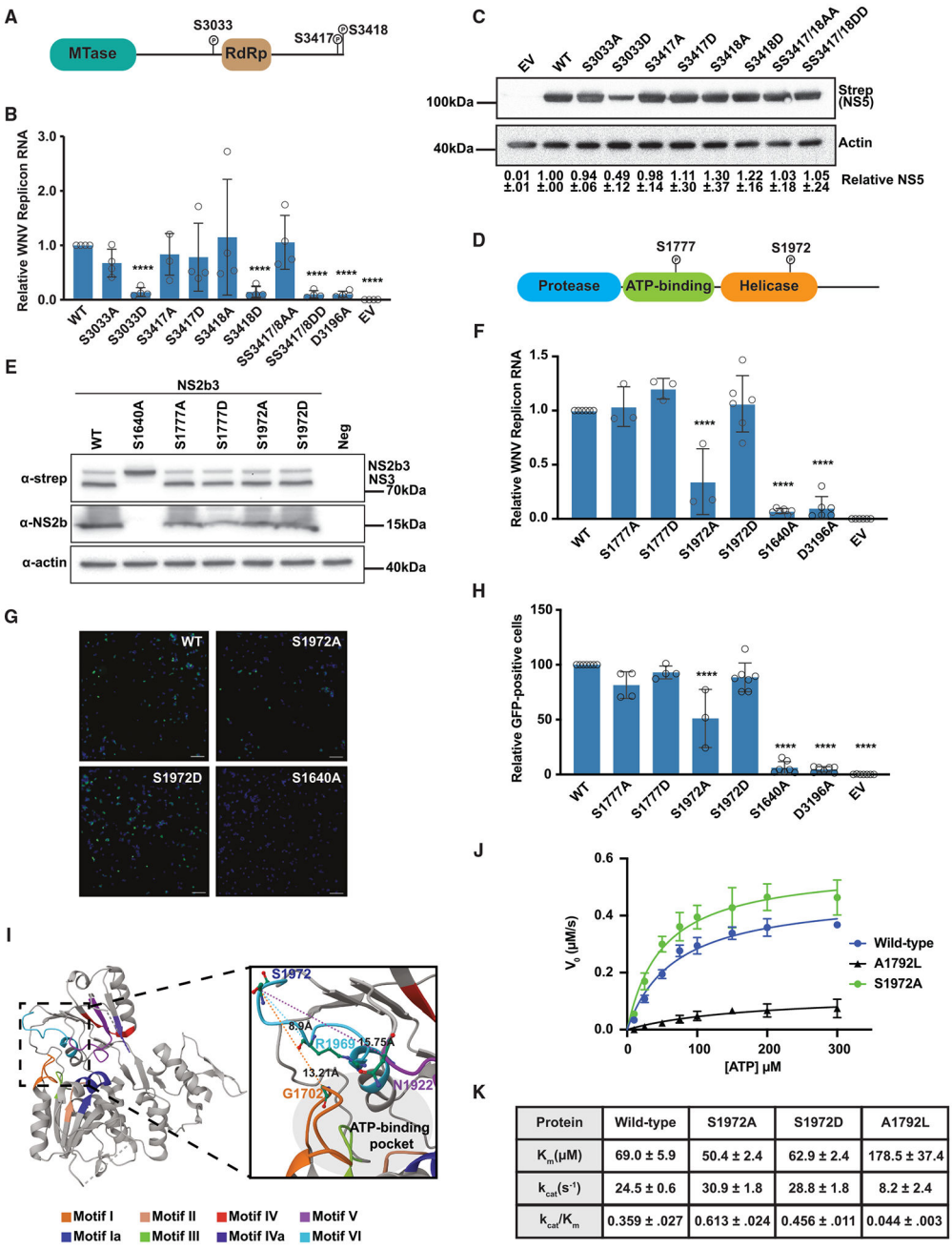

Protein	Wild-type	S1972A	S1972D	A1792L
K_m(μM)	69.0 ± 5.9	50.4 ± 2.4	62.9 ± 2.4	178.5 ± 37.4
k_{cat}(s^{-1})	24.5 ± 0.6	30.9 ± 1.8	28.8 ± 1.8	8.2 ± 2.4
k_{cat}/K_m	0.359 ± .027	0.613 ± .024	0.456 ± .011	0.044 ± .003

Figure 4. Characterization of phosphorylation sites on WNV NS3 and NS5 proteins

(A) WNV NS5 schematic with phosphorylated residues indicated.

(B) Wild-type (WT) or mutant WNV replicon constructs were transfected into HEK293T cells; relative WNV replicon RNA is normalized to the WT control. The RdRp-dead D3196A and empty vector (EV) are included as controls. $n = 4$.

(C) Representative western blot of strep-tagged WT and phospho-mutant WNV NS5 with actin loading control. Relative protein expression (Alphaview) is indicated underneath each lane, mean ± SE. $n = 4$.

(D) WNV NS3 schematic with phosphorylated residues indicated.
(E) Western blot demonstrating self-cleavage of strep-tagged NS2b/3 constructs with actin as a loading control. The NS3 protease-dead (S1640A) construct is included as a control.
(F) A replicon assay was performed as described in (B). The S1640A mutant is included as a control. $n = 3–6$.
(G) Representative immunofluorescence images from data quantified in (H). Hoechst (DNA) is shown in blue, GFP in green, scale bar indicates 150 μm.
(H) Quantification of WT-normalized GFP^+ HEK293T cells following transfection of the indicated WNV replicons. S1640A, D3196A, and EV are included as controls. $n = 3–7$.
(I) Structure of the WNV NS3 helicase domain (PDB: 2QEQ) with motifs false colored and ATP-binding pocket in gray.
(J) Michaelis-Menten kinetic curves for WT, A1792L, and S1972A NS3h.
(K) K_m and k_{cat} ± SE and catalytic efficiency (k_{cat}/K_m) ± SE for each mutant. $n = 3–5$.
Unless indicated, the mean ± SD is shown for all data. Western blot data are representative of ≥2 independent experiments. Statistics are one-way ANOVA with corrections for multiple comparisons; ****$p < 0.0001$. See also Figures S4 and S5.

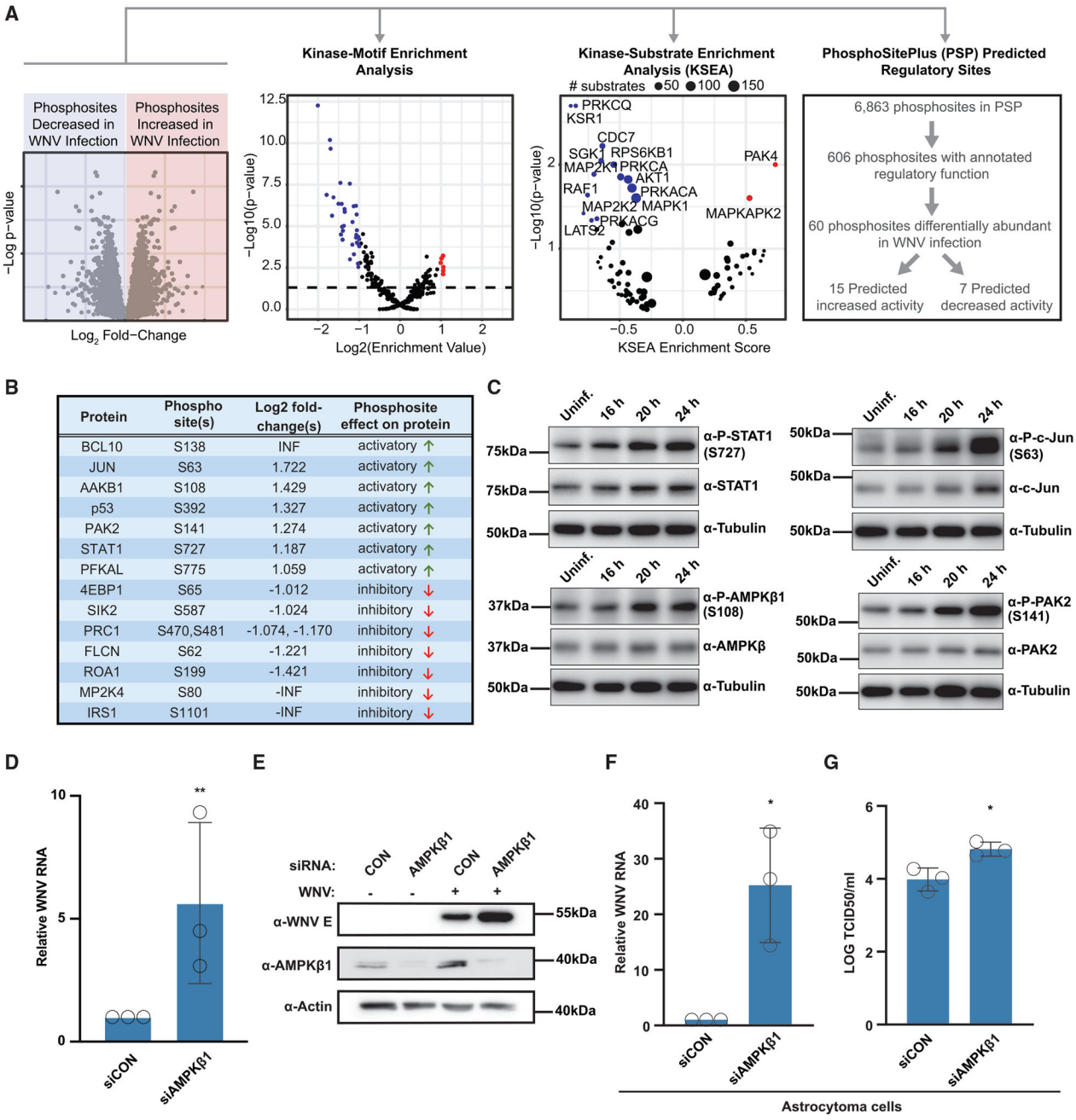

Protein	Phospho site(s)	Log2 fold-change(s)	Phosphosite effect on protein
BCL10	S138	INF	activatory ↑
JUN	S63	1.722	activatory ↑
AAKB1	S108	1.429	activatory ↑
p53	S392	1.327	activatory ↑
PAK2	S141	1.274	activatory ↑
STAT1	S727	1.187	activatory ↑
PFKAL	S775	1.059	activatory ↑
4EBP1	S65	-1.012	inhibitory ↓
SIK2	S587	-1.024	inhibitory ↓
PRC1	S470,S481	-1.074, -1.170	inhibitory ↓
FLCN	S62	-1.221	inhibitory ↓
ROA1	S199	-1.421	inhibitory ↓
MP2K4	S80	-INF	inhibitory ↓
IRS1	S1101	-INF	inhibitory ↓

Figure 5. Protein phosphorylation during WNV infection

(A) Significantly changed phosphorylated peptides were analyzed by: (left) Kinase Library analysis with volcano plot showing increased (red) or decreased (blue) consensus motifs in WNV-infected cells for indicated kinases; (middle) kinase-substrate enrichment analysis (KSEA), with increased (red) or decreased (blue) kinase substrates during infection; and (right) differentially abundant phosphosites in WNV infection with an annotated regulatory function (PhosphoSitePlus).

(B) Regulatory phosphosites predicted to increase activity during infection.

(C) Validation of phosphorylation by western blot in WNV-infected U2OS cells (NY2000, MOI 1), with tubulin shown as a loading control.
(D) Relative WNV RNA following infection upon AMPKβ1 depletion in U2OS cells, normalized to siControl (siCON).
(E) Silenced U2OS cells were infected with WNV NY2000 (MOI 10) and lysates were probed with the indicated antibodies.
(F) Relative WNV NY2000 RNA from silenced CCF-STTG1 astrocytoma cells. Infections are normalized as in (D).
(G) $TCID_{50}$ assays were performed on supernatants from (F). Data are presented as $\log10(TCID_{50}/mL)$.
For all data, the mean ± SD is shown. $n = 3$. Western blot data are representative of ≥2 independent experiments. Significance is indicated by $*p < 0.05$ or $**p < 0.005$, two-tailed Student's t test. See also Figure S6; Tables S7, S8, and S9.

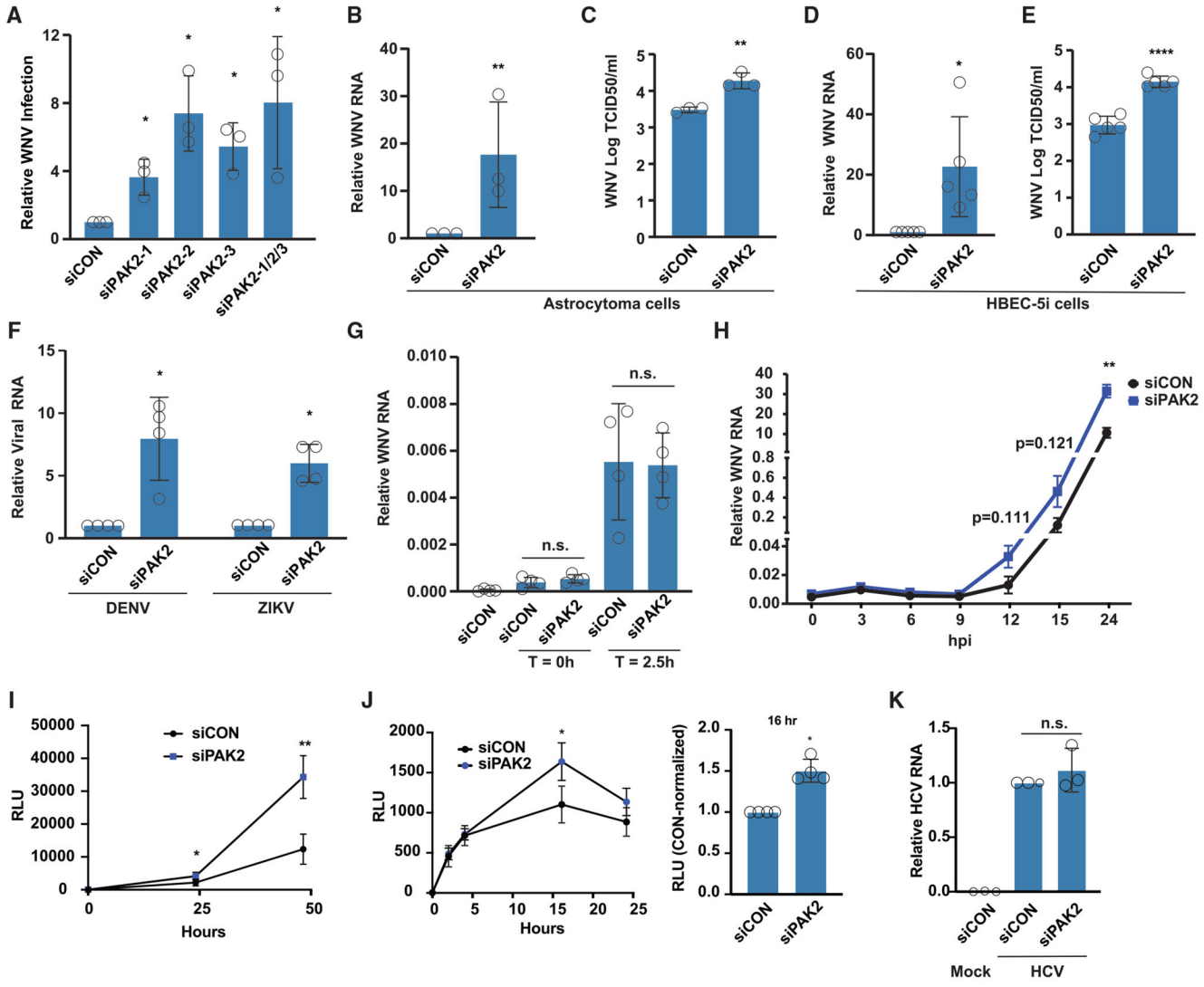

Figure 6. PAK2 restricts WNV by inhibiting viral RNA translation

(A) U2OS cells were transfected with PAK2 siRNAs and infected with WNV NY2000. Relative WNV RNA is normalized to cells treated with siControl (siCON). $n = 3$.

(B) Relative WNV RNA from PAK2-silenced CCF-STTG1 cells. Data are normalized as in (A). $n = 3$.

(C) Supernatant from (B) was used to perform $TCID_{50}$ assays. Data shown are the mean ± SD log10($TCID_{50}$/mL). $n = 3$.

(D) Relative WNV RNA from infected HBEC-5i cells transfected as in (B), normalized to siCON samples. $n = 5$.

(E) $TCID_{50}$ assays were performed on supernatants from (D). Data shown are the mean ± SD log10($TCID_{50}$/mL). $n = 5$.

(F) Relative DENV and ZIKV RNA from U2OS cells transfected with PAK2 siRNAs. Data are normalized as in (A). $n = 4$.

(G) Viral entry of WNV NY2000 in PAK2-silenced U2OS cells. $n = 4$.

(H) Relative viral RNA from PAK2-silenced U2OS cells at indicated time points. $n = 4$.

(I) PAK2-silenced HEK293T cells were transfected with *Renilla* luciferase DENV replicon RNA. $n = 4$.

(J) PAK2-silenced HEK293T cells were transfected with a capped polymerase-dead DENV replicon RNA. $n = 4$.

(K) Relative viral RNA from PAK2-silenced Huh7.5 cells infected with hepatitis C virus (HCV) for 24 h, normalized to siCON. $n = 3$.

For all data, the mean ± SD is shown. All analyses are either two-tailed unpaired Student's t test or one-way ANOVA with corrections for multiple comparisons. n.s. indicates $p > 0.05$; *$p < 0.05$, **$p < 0.01$, and ****$p < 0.0001$. See also Figure S7.

KEY RESOURCES TABLE

REAGENT or RESOURCE	SOURCE	IDENTIFIER
Antibodies		
Mouse monoclonal anti-Strep tag II	Abcam	Cat# ab184224, RRID:AB_3086746
Mouse monoclonal anti-Tubulin (clone DM1A)	Sigma	Cat# T6199, RRID:AB_477583
Rabbit polyclonal anti-WNV NS2b	Genetex	Cat# GTX132060, RRID:AB_2886552
Rabbit polyclonal anti-beta Actin	Cell Signaling Technology	Cat# 4967, RRID:AB_330288
Rabbit monoclonal anti-Rig-I (clone D14G6)	Cell Signaling Technology	Cat# 3743, RRID:AB_2269233
Rabbit monoclonal anti-CD44 (clone E7K2Y)	Cell Signaling Technology	Cat# 37259, RRID:AB_2750879
Rabbit polyclonal anti-RAP1B	Genetex	Cat# GTX111933, RRID:AB_1951632
Rabbit polyclonal anti-Ubiquitin	Enzo	Cat# ADI-SPA-200
Rabbit polyclonal anti-LC3	ProteinTech	Cat# 14600-1-AP, RRID:AB_2137737
Rabbit monoclonal anti-MEK1/2 (clone D1A5)	Cell Signaling Technology	Cat# 8727, RRID:AB_10829473
Rabbit monoclonal anti-Histone H3 (Clone D1H2)	Cell Signaling Technology	Cat# 4499, RRID:AB_10544537
Rabbit polyclonal anti-STAT1-pS727	Cell Signaling Technology	Cat# 9177 RRID:AB_2197983
Rabbit polyclonal anti-STAT1	Cell Signaling Technology	Cat# 9172 RRID:AB_2198300
Rabbit polyclonal anti-c-Jun-pS63	Cell Signaling Technology	Cat# 9261 RRID:AB_2130162
Rabbit monoclonal anti-c-Jun (clone 60A8)	Cell Signaling Technology	Cat# 9165 RRID:AB_2130165
Rabbit polyclonal anti-PAK2-pS141	Cell Signaling Technology	Cat# 2606 RRID:AB_2299279
Rabbit polyclonal anti-PAK2	Cell Signaling Technology	Cat# 2608 RRID:AB_2283388
Rabbit polyclonal anti-WNV Envelope	Genetex	Cat# GTX132052, RRID:AB_2886550
Rabbit polyclonal anti-AMPKα-pThr172	Cell Signaling Technology	Cat# 2531 RRID:AB_330330
Rabbit polyclonal anti-AMPKα	Cell Signaling Technology	Cat# 2532 RRID:AB_330331
Rabbit polyclonal anti-AMPKβ1-pS108	Abcam	Cat# ab156890
Rabbit polyclonal anti-AMPKβ1	Cell Signaling Technology	Cat# 12063 RRID:AB_2797812
Rabbit polyclonal anti-ACC	Cell Signaling Technology	Cat# 3662 RRID:AB_2219400
Rabbit polyclonal anti-ACC-pS79	Cell Signaling Technology	Cat# 3661 RRID:AB_330337
Rabbit monoclonal anti-TBK1 (clone D1B4)	Cell Signaling Technology	Cat# 3504 RRID:AB_2255663
Rabbit monoclonal anti-TBK1 pS172 (clone D52C2)	Cell Signaling Technology	Cat# 5483 RRID:AB_10693472
Mouse monoclonal anti-WNV Env (clone 4G2)	Dr. Michael Diamond	N/A
Goat polyclonal anti-Rb IgG-AF488	Thermofisher	Cat# A-11034 RRID:AB_2576217
Goat polyclonal Anti-Ms IgG-AF488	Thermofisher	Cat# A-11029 RRID:AB_2534088
Goat polyclonal Anti-Rb IgG-HRP	Thermo Scientific	Cat# G-21234 RRID:AB_2536530
Goat polyclonal Anti-Ms IgG-HRP	Thermo Scientific	Cat# G-21040 RRID:AB_2536527
Bacterial and virus strains		
Stellar DH5α	TakaraBio	636763
STBL2 competent *E. coli*	Thermo Scientific	10268019
West Nile Virus Kunjin CH16532	World Reference Center of Emerging Viruses and Arboviruses	N/A

REAGENT or RESOURCE	SOURCE	IDENTIFIER
West Nile virus NY2000 Crow 3356	Dr. Michael Diamond	N/A
DENV2 NGC	BEI Resources	N/A
ZIKV Mexico 2016 Mex2-81	World Reference Center of Emerging Viruses and Arboviruses	N/A
Biological samples		
N/A	N/A	N/A
Chemicals, peptides, and recombinant proteins		
Eeyarestatin	Tocris	Cat# 3922
LS-102	EMD Millipore	Cat# 5.38184.0001
MG-132	EMD Millipore	Cat# 474787
Bortezomib	EMD Millipore	Cat# 5.04314.0001
Bafilomycin A1	Cell Signaling Technology	Cat# 54645
Critical commercial assays		
Renilla-Glo luciferase assay	Promega	Cat# E2720
PowerUp SYBR green	Thermo Scientific	Cat# A25743
Deposited data		
Proteomics data	ProteomeXchange Consortium-PRIDE repository	PXD050159
Experimental models: Cell lines		
U2OS	ATCC	HTB-96
HEK293T	ATCC	CRL-3216
BHK-21	ATCC	CCL-10
CCF-STTG1	ATCC	CRL-1718
C6/36	ATCC	CRL-1660
HBEC-5i	ATCC	CRL-3245
Oligonucleotides		
siRNAs: See Table S11 for full list	N/A	N/A
Cloning primers: See Table S10 for full list	N/A	N/A
qPCR primers: See Table S13 for full list	N/A	N/A
Recombinant DNA		
Overexpression screen vectors: See Table S6	N/A	N/A
Plasmids: See Table S12	N/A	N/A
Software and algorithms		
ImageJ (FIJI) v2.16.0/1.54p	https://imagej.net/ij/download.html	N/A
Alphaview v3.5.0.927	Bio-Techne	N/A
MaxQuant v1.6.8.0	https://www.maxquant.org/	N/A
MSStats v3.22.1	Bioconductor	N/A
ClustalOmega v1.2.4	https://www.ebi.ac.uk/jdispatcher/msa/clustalo	N/A
Morpheus v1.0.15	https://software.broadinstitute.org/morpheus/	N/A
Other		

REAGENT or RESOURCE	SOURCE	IDENTIFIER
R code for proteomics analysis	Github	https://github.com/jrjohns1/Walter-et-al